Chemical Geology 502 (2018) 1–14

Contents lists available at ScienceDirect

Chemical Geology

journal homepage: www.elsevier.com/locate/chemgeo

VSI: ConwayGEOTRACES

Concentrations, provenance and flux of aerosol trace elements during US GEOTRACES Western Arctic cruise GN01☆

Chris M. Marsay[a], David Kadko[b], William M. Landing[c], Peter L. Morton[d], Brent A. Summers[c,1], Clifton S. Buck[a,*]

[a] Skidaway Institute of Oceanography, University of Georgia, 10 Ocean Science Circle, Savannah, GA 31411, USA
[b] Florida International University, Applied Research Center, 10555 West Flagler St., Miami, FL 33174, USA
[c] Department of Earth, Ocean and Atmospheric Science, Florida State University, Tallahassee, FL 32306, USA
[d] National High Magnetic Field Laboratory, 1800 E. Paul Dirac Dr., Tallahassee, FL 32310, USA

ARTICLE INFO

Editor: Catherine C

Keywords:
Aerosol
Trace element
Arctic
^{7}Be
GEOTRACES
Atmospheric deposition

ABSTRACT

The Arctic region is undergoing significant changes in climate, with a notable decrease in summertime sea ice coverage over the past three decades. This trend means an increasing proportion of Arctic Ocean surface waters can receive direct deposition of material from the atmosphere, potentially influencing marine biogeochemical cycles and delivery of pollutants to the Arctic ecosystem. Here, we present aerosol concentrations of selected trace elements (Al, Ti, V, Mn, Fe, Co, Ni, Cu, Zn, Cd, and Pb) measured during the US GEOTRACES Western Arctic cruise (GN01, also known as HLY1502) in August–October 2015. Concentrations of "lithogenic" elements (Al, Ti, V, Mn, Fe, and Co) were similar to those measured in remote and predominantly marine-influenced air masses in previous studies, reflecting the remoteness of the Arctic Ocean from major dust sources. Concentrations of Ni, Cu, Zn, Pb, and Cd showed significant enrichments over crustal values, and were often of similar magnitude to concentrations measured over the North Atlantic in air masses of North American or European provenance. We use ^{7}Be inventory and flux data from GN01 to estimate a bulk atmospheric deposition velocity during the study period, and combine it with our aerosol concentrations to calculate atmospheric deposition fluxes of the trace elements in the Arctic region during late summer. The resulting estimates for mineral dust and Fe deposition fall at the low end of global estimates and confirm the Arctic Ocean as a low-dust environment during the summer months.

This article is part of a special issue entitled: Conway GEOTRACES - edited by Tim M. Conway, Tristan Horner, Yves Plancherel, and Aridane G. González.

1. Introduction

Atmospheric transport of dust from the continents and its eventual deposition to the ocean is an important input of many bioactive trace elements (TEs; e.g. Fe, Mn, Co, Ni, Zn, Cd) to surface waters remote from the influences of continental runoff and shelf inputs (Duce et al., 1991; Jickells et al., 2005). The same atmospheric transport process can deliver significant anthropogenic contributions of certain elements (e.g. V, Cu, Zn, Cd, Pb) to areas of the ocean distant from their emission sources (Arimoto et al., 1995; Guo et al., 2014; Helmers and Rutgers van der Loeff, 1993), resulting in considerable perturbations from the natural supply rate for some of these elements (Pacyna and Pacyna, 2001). Sea-salt particles, formed by wind action at the air-sea interface, natural and anthropogenic biomass burning, and particles released by volcanic emissions also contribute to the atmospheric transport of trace elements (Arimoto et al., 2003; Cottle et al., 2014; Duggen et al., 2010; Jones and Gislason, 2008).

Mineral dust deposited to the surface ocean also acts as mineral ballast that increases the sinking speed of marine organic particles, and can scavenge trace elements from the water column (Armstrong et al., 2002; Ittekkot, 1993; Rogan et al., 2016). However, total annual dust deposition flux varies region-to-region by more than two orders of magnitude (Mahowald et al., 2005), implying that its influence on surface ocean biogeochemistry differs significantly over global scales (e.g. Boyd et al., 2010). In the polar regions, aerosol deposition onto snow and ice can also result in a lowering of the surface albedo, and

☆ This article is part of a special issue entitled: Conway GEOTRACES - edited by Tim M. Conway, Tristan Horner, Yves Plancherel, and Aridane G. González.

* Corresponding author.
E-mail address: clifton.buck@skio.uga.edu (C.S. Buck).
[1] Now at: College of Marine Science, University of South Florida, St. Petersburg, FL 33701, USA.

https://doi.org/10.1016/j.chemgeo.2018.06.007
Received 29 November 2017; Received in revised form 8 May 2018; Accepted 11 June 2018
Available online 18 June 2018
0009-2541/

therefore influence the radiative budget (Law and Stohl, 2007).

Model simulations indicate that atmospheric dust deposition to the Arctic Ocean falls at the low end of global atmospheric fluxes, averaging $< 0.5\,g\,m^{-2}\,y^{-1}$, due to a lack of proximal major dust sources (Jickells et al., 2005; Mahowald et al., 2005). Observations support the models, with relatively low particle numbers and low concentrations of aerosol Al (a proxy for mineral dust) measured at land-based stations around the edges of the Arctic Ocean (Gong and Barrie, 2005; Hirdman et al., 2010; Rahn, 1981; Tunved et al., 2013), and by the few shipboard measurements made in the Arctic Ocean (Kadko et al., 2016; Lannefors et al., 1983; Maenhaut et al., 1996). However, compositional studies of Arctic aerosols have shown significant enrichments of several TEs over crustal values due to contributions from anthropogenic emissions transported from further south, and particularly related to industrial processes in northern Eurasia and Siberia (Gong and Barrie, 2005; Kadko et al., 2016; Shevchenko et al., 2003; Stohl, 2006).

Time-series studies have revealed a strong seasonal cycle in Arctic aerosol concentrations, with highest concentrations in the winter and spring, when maxima in pollutant aerosols contribute to “Arctic haze” (Shaw, 1995; Zhan and Gao, 2014). This phenomenon results largely from meteorological factors rather than seasonal changes in emissions in the Arctic region itself. During winter, low pressure systems over the northern Atlantic and Pacific Oceans – the Icelandic Low and the Aleutian Low – act as conduits to transport pollutants into the Arctic. These anthropogenic aerosols include sulfate, black carbon, and heavy metals from fossil fuel combustion and other industrial sources, primarily in Eurasia and North America (Barrie, 1986; Hirdman et al., 2010; Macdonald et al., 2005). This input of pollutants is exacerbated by the stable, cold troposphere over the wintertime Arctic, and the associated low rate of precipitation, resulting in relatively long aerosol residence times and a consequent build-up of the pollutant aerosols (Barrie, 1986; Shaw, 1995). In contrast, during the summer months, atmospheric transport from lower latitudes is diminished due to northward recession of the Polar Front, leaving the Arctic troposphere more isolated from industrial sources, and there is also more efficient scavenging of particles from the lower atmosphere by more frequent precipitation (Barrie, 1986; Stohl, 2006). Together, this results in a shorter residence time of atmospheric particles and a minimum in aerosol concentrations in late summer (Hirdman et al., 2010; Tunved et al., 2013).

There are relatively few studies of TEs in aerosols over the central Arctic Ocean. Kadko et al. (2016) reported concentration data for multiple elements from aerosols collected north of 80°N during three short sampling periods in August–September 2011, while Maenhaut et al. (1996) reported median atmospheric concentrations of multiple elements from samples collected in the Nansen and Amundsen Basins in August–October 1991. Shevchenko et al. (2003) summarized atmospheric concentrations of some trace elements from a number of mostly-summertime expeditions in the Russian Arctic. Measurements of multiple elements in aerosol samples collected at land-based sites around the Arctic Ocean indicate that, as with non-sea-salt sulfate, TEs with significant anthropogenic sources (Ni, Cu, Zn, Pb) have strong seasonality, with maxima in late winter/early spring (Barrie and Hoff, 1985; Gong and Barrie, 2005; Laing et al., 2014a). In contrast, concentrations of soil-related TEs (Al, Fe, Mn) display weak seasonality at Alert, Canada (82.5°N, 62.3°W), with one small maximum in late spring, due to long range dust transport, and another in late summer due to local sources. Boreal forest fires in Siberia and North America can also have a noticeable effect on aerosol optical depth and black carbon concentrations in the Arctic during summer months (Hirdman et al., 2010; Stohl et al., 2006) and may also influence atmospheric concentrations and deposition of some elements, while volcanic eruptions, particularly in the Aleutian Islands and on the Kamchatka Peninsula, also have the potential to influence Arctic aerosol TE concentrations.

Studies of trace element biogeochemistry in the Arctic Ocean and the impacts of atmospheric inputs are currently limited. It is thought that atmospheric deposition of the key micronutrient iron represents a minor input, relative to inputs from the surrounding continental shelves and Eurasian rivers, the influence of which reach the central basin through the Transpolar Drift and the sea ice that it transports (Klunder et al., 2012; Wang et al., 2014). Nonetheless, Klunder et al. (2012) documented lower dissolved Fe concentrations outside of the area influenced by the Transpolar Drift, while Taylor et al. (2013) reported dissolved Fe concentrations low enough to co-limit primary production in the Beaufort Sea.

Reduced sea-ice coverage during the summer months allows more direct input of atmospheric TEs to Arctic Ocean surface waters during this season. In contrast, winter deposition takes place predominantly onto snow and ice and may be modified by photochemical reactions as well as by processing through melt ponds during the following spring melt before it reaches surface waters. How these respective input pathways influence the bioavailability of atmospherically supplied materials remains an open question. The current warming trend, with earlier seasonal melting and more extensive areas of open water (Comiso, 2012; Vaughan et al., 2013), underscores the importance of quantifying the summertime atmospheric deposition to the Arctic Ocean to assess its impact on marine biogeochemical cycles of TEs and the carbon cycle.

The aims of this paper are: (1) to add aerosol TE concentration data collected during late summer/early fall as part of the 2015 US GEOTRACES Western Arctic Section to the small dataset of aerosol TE measurements currently available for the Arctic Ocean and compare these to land-based Arctic aerosol studies and measurements made in other oceanic regions; (2) to discuss aerosol provenance and enrichment of TEs in aerosols collected during the GEOTRACES cruise; and (3) to estimate the summertime atmospheric deposition flux of TEs to the Arctic in order to improve our understanding of the biogeochemical cycles of these elements in the region.

2. Methods

2.1. Sample collection

A total of fourteen multi-day integrated aerosol samples were collected during the US GEOTRACES Western Arctic research cruise (hereafter known as GN01), which took place from 9th August to 12th October 2015 on the USCGC *Healy* (cruise HLY1502). The cruise track consisted of a northward transect from Dutch Harbor, Alaska, across the Bering Sea, through the Bering Strait and across the Makarov Basin to the North Pole, followed by a return transect across the Canada Basin and back across the Bering Sea to Dutch Harbor (Fig. 1, with deployment locations of aerosol samples Aer01 to Aer14 shown).

Bulk aerosol samples for multiple trace element analyses were collected using one of five Tisch Environmental high-volume ($\sim$1 m^3 air min^{-1}) aerosol samplers (model 5170V-BL). For each deployment, 12 replicate 47 mm diameter Whatman 41 filters were loaded on open-face filter holders (Advantec MFS) installed on the aerosol sampler upon a PVC adaptor plate (Shelley et al., 2015). Filters were acid-washed before use to reduce trace element blanks, following the procedure described by Morton et al. (2013). The samplers were deployed on the ship's flying bridge ($\sim$23 m above sea level) to minimize the influence of sea spray on samples. In order to eliminate contamination from the ship's stack exhaust, samplers were deployed as far forward of the stack as possible, and controlled by wind speed and direction through a Campbell Scientific CR800 data-logger, interfaced with an anemometer and wind vane set up in close proximity to the samplers. This setup was used to restrict sampling to periods when relative wind speed and direction were $> 0.5\,m\,s^{-1}$ and from within $\pm$ 60° of the bow of the ship, respectively, for at least five continuous minutes.

Due to the relatively low frequency of in-sector wind conditions, and the low dust concentrations expected in the Arctic Ocean, filters

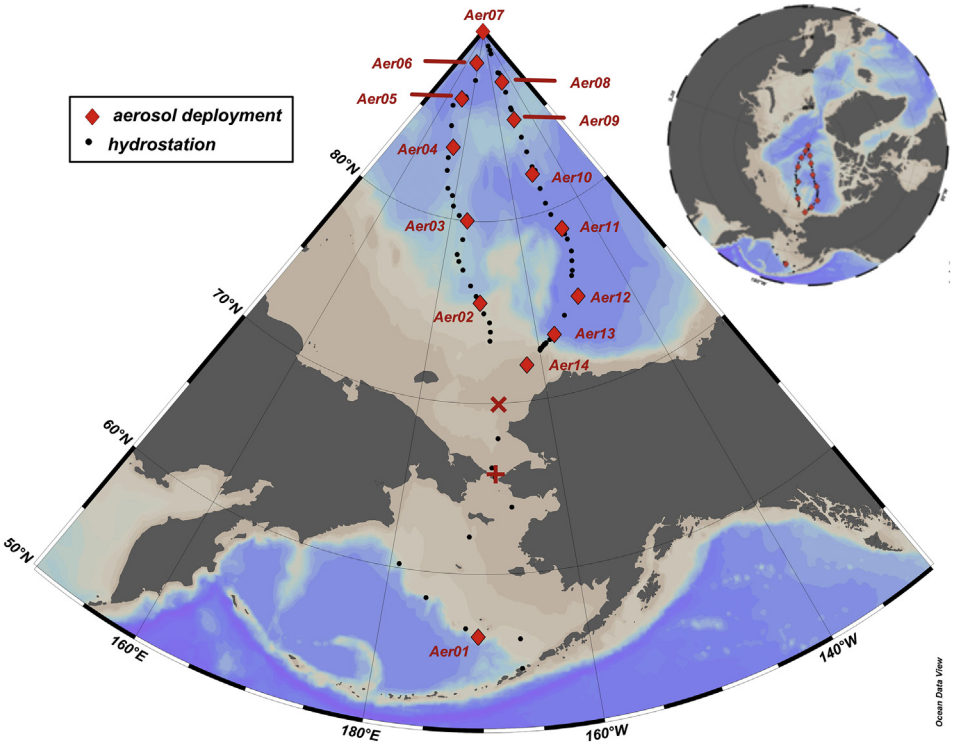

Fig. 1. Map showing locations of aerosol deployments (red diamonds) along the GN01 cruise track, and the locations of hydrostations (black dots). The recovery location of each aerosol sample coincided roughly with the deployment location for the following sample with the exceptions of Aer01 (recovery location shown by red 'x') and Aer14 (shown by red '+'). (For interpretation of the references to color in this figure legend, the reader is referred to the web version of this article.)

were typically deployed for 3–4 days before being replaced (Table 1). The volume of air filtered through each set of filters averaged 2224 m^3 (equal to 185 m^3 through each filter), and ranged from 154 to 6717 m^3 (13–560 m^3 per filter; Table 1). Total sampling time (and therefore volume of air filtered) during the first sample is uncertain due to power problems that affected the digital timer of the aerosol sampler, and so the volume of air sampled for Aer01 in Table 1 is a best estimate value from "in-sector" conditions, along with a maximum possible uncertainty. Filters were transferred to plastic petri dishes after recovery, and stored frozen prior to processing upon return to the laboratory. All filter loading and unloading to/from the PVC adaptors was carried out in a laminar flow bench, located within a plastic "bubble" constructed in the ship's main laboratory and supplied with HEPA-filtered air.

Additional triplicate aerosol samples for ^{7}Be analysis were collected on 47 mm Whatman 41 filters loaded on a separate high-volume sampler with the same sector controls during a subset of filter deployments (Aer04, Aer06, Aer07, Aer09, Aer10, and Aer11). Bulk deposition (dry deposition and snowfall) samples for ^{7}Be analysis were also collected, by collecting volumes of snow down to the snow-ice boundary (9–12 cm depth; 1 m^2 area) from the sea ice at six ice stations, and by using 21 cm diameter buckets deployed close to the aerosol samplers on the ship's flying bridge (Table 2).

2.2. Sample processing and analysis

To determine total TE concentrations of the samples, filters were subjected to a three-stage strong acid digestion, carried out in a Class-1000 clean room and following the method of Morton et al. (2013). Briefly, filters were transferred to individual 15 mL Teflon vials (Savillex), and digested successively with 1 mL concentrated quartz-distilled HNO_3 (Q-HNO_3), followed by 0.5 mL concentrated Q-HNO_3 and 0.1 mL concentrated HF (Fisher Optima), and finally 0.5 mL concentrated Q-HNO_3. At each stage, samples were heated at 150 °C overnight and taken to dryness the following day. After the final dry-down, samples were redissolved in 4 mL of 0.32 M Q-HNO_3 for analysis. For every third sample, triplicate filters from the same aerosol sampler

Table 1
Aerosol sample deployment and recovery information, with volume of air sampled per filter. All dates and times are in Universal Coordinated Time (UTC).

Sample	Start date & time	Latitude (°N)	Longitude (°W)	End date & time	Latitude (°N)	Longitude (°W)	Air volume per filter (m^3)
Aer01	10 Aug 2015 17:53	56.07	170.51	17 Aug 2015 17:15	69.93	167.69	559.7 ± 115.4[a]
Aer02	20 Aug 2015 05:34	75.57	170.75	23 Aug 2015 18:12	80.00	174.95	173.7
Aer03	23 Aug 2015 19:21	80.00	174.96	27 Aug 2015 16:19	83.57	−174.73	270.4
Aer04	27 Aug 2015 20:49	83.76	−175.04	30 Aug 2015 21:40	86.24	−170.65	116.0
Aer05	30 Aug 2015 23:57	86.36	−171.69	04 Sep 2015 02:42	88.40	−176.64	12.8
Aer06	04 Sep 2015 10:02	88.41	−176.75	08 Sep 2015 04:34	89.94	97.85	275.6
Aer07	08 Sep 2015 06:05	89.94	104.19	12 Sep 2015 03:45	87.35	149.43	118.4
Aer08	12 Sep 2015 06:13	87.27	149.04	16 Sep 2015 04:30	85.15	149.85	72.7
Aer09	17 Sep 2015 00:20	85.16	150.40	20 Sep 2015 22:13	82.26	149.38	102.9
Aer10	21 Sep 2015 01:10	82.10	150.81	26 Sep 2015 03:05	78.97	148.50	321.3
Aer11	26 Sep 2015 04:38	78.80	148.09	29 Sep 2015 19:34	75.05	150.18	116.6
Aer12	29 Sep 2015 20:31	75.06	150.21	03 Oct 2015 16:25	73.43	156.79	211.8
Aer13	03 Oct 2015 18:41	73.40	156.77	07 Oct 2015 17:33	72.00	162.56	152.2
Aer14	07 Oct 2015 18:40	72.00	162.56	09 Oct 2015 23:50	65.95	168.45	90.5

[a] Total sampling time during the first sample is uncertain due to power problems, so the volume of air sampled for Aer01 is a best estimate from "in sector" conditions, along with a maximum possible uncertainty.

Table 2
Atmospheric ^{7}Be flux calculated from (a) snow samples collected on sea-ice and from (b) bulk deposition samples collected in buckets deployed on the flying bridge. All dates are UTC.

(a)

Station	Latitude (°N)	Longitude (°W)	Snow start date	Collection date	*t* (days)[a]	^{7}Be activity (dpm m^{-2})[b]	^{7}Be flux (dpm m^{-2} d^{-1})[c]
31	88.41	176.76	08/23/15	09/04/15	12	469	42.23
33	89.99	−89.25	08/23/15	09/07/15	15	425	31.16
39	87.77	148.71	08/23/15	09/11/15	19	778	46.19
42	85.72	150.61	08/23/15	09/14/15	22	513	26.81
43	85.16	149.97	08/23/15	09/16/15	24	809	39.25
46	82.50	149.79	08/23/15	09/19/15	27	319	14.03
						Mean ± 1SD	33.3 ± 10.8

(b)

Sample	Deployment date	Recovery date	*t* (days)[a]	^{7}Be activity (dpm m^{-2})[d]	^{7}Be flux (dpm m^{-2} d^{-1})[c]
Bucket 1 stbd.	09/01/15	09/18/15	17	457	29.9
Bucket 1 port	09/01/15	09/18/15	17	314	20.6
Bucket 2 port	09/18/15	10/07/15	19	723	42.95
Bucket-DH stbd.	10/02/15	10/11/15	9	731	86.1
				Mean ± 1SD	44.9 ± 29.0

[a] Time between snow onset and sample collection, or deployment duration of sample buckets.
[b] Measured ^{7}Be in 1 m^{2} of snow.
[c] Calculated from Eq. (5).
[d] Measured ^{7}Be normalized to bucket area.

were processed to assess the homogeneity of material collected on the twelve replicate filters. Blank filters were treated in exactly the same way as samples and average blank values were subtracted from each sample. The suitability of this digestion method for measuring Al, Ti, V, Fe, Zn, and Pb has been evaluated previously by application to certified reference materials (Morton et al., 2013). Additional application of the method to PACS-2 certified reference material (marine sediment; National Research Council of Canada) during this study gave mean recoveries (n = 5) of 99% (Al), 100% (Ti), 105% (V), 97% (Mn), 101% (Fe), 103% (Co), 89% (Ni), 99% (Cu), 108% (Zn), 89% (Cd), and 77% (Pb).

Determinations of total aerosol trace elements were made on a high-resolution inductively coupled mass spectrometer (HR-ICPMS; Thermo-Element 2) at the National High Magnetic Field Laboratory at Florida State University. Solutions resulting from blank filter and sample filter digests were drift-corrected using an internal In standard (10 ppb; High Purity Standards) and the elemental concentrations quantified using multi-element external calibration standards (High Purity Standards) in low resolution and medium resolution modes. All bulk aerosol TE concentrations from GN01 are publically available at the Biological and Chemical Oceanography Data Management Office (BCO-DMO) online data repository (www.bco-dmo.org/dataset/725905).

Aerosol and snow samples for ^{7}Be analysis were treated as described in Kadko et al. (2016). Briefly, three 47 mm Whatman 41 aerosol sample filters were stacked together in a plastic Petri dish and counted for ^{7}Be. This configuration was calibrated with a commercially prepared mixed solution of known gamma activities. Snow and bulk deposition samples were melted and received 5 mL of concentrated HCl, 5 mL of $FeCl_3$ in solution, and 0.5 mL of a stable Be tracer. After 12 h of equilibration, a concentrated NaOH solution was slowly added to co-precipitate the ^{7}Be with $Fe(OH)_3$. The precipitate was returned to the lab where it was dried, placed in Petri dishes, and counted by gamma spectroscopy calibrated for this geometry. The precipitate was redissolved in dilute HCl, and analyzed for stable Be by atomic adsorption to calculate recovery yields.

2.3. Air mass back trajectory analysis

The publicly available NOAA Air Resources Laboratory HYbrid Single-Particle Lagrangian Integrated Trajectory (HYSPLIT) model (Rolph et al., 2017; Stein et al., 2015) was used to calculate three-day (72 h) air mass back trajectories for the air masses arriving at the deployment and recovery dates and locations for each sample (Fig. S1). The ensemble trajectory option of HYSPLIT with the Global Data Assimilation System (GDAS) and 1° global meteorology data set was used. An arrival height of 300 m was chosen, and comparisons with back trajectories carried out with arrival heights of 50 m and 500 m (both within the marine boundary layer) did not show large differences over the 3-day trajectory period. Due to the 3–5 day deployment times for each sample, additional back trajectory analyses were run using as the arrival location any hydrographic stations that were occupied during each aerosol deployment interval in an effort to identify any significant changes in air mass influence.

3. Results and discussion

3.1. Trace element concentrations in aerosol samples

The atmospheric loadings of Al, Ti, V, Mn, Fe, Co, Ni, Cu, Zn, Cd, and Pb, in pmol m^{-3}, are shown in Fig. 2 for all samples except Aer05. The Aer05 sample was recovered four days after deployment, but consisted of only 2 h of sampling time and only 12.8 m^{3} of air having passed through each filter, due to unsuitable wind conditions and problems with the sampler motor. At recovery, visual inspection of filters from all deployments indicated very low aerosol loading, with little or no difference in color discernible between exposed parts of the filters and the filter edges. Trace element concentrations in sample digests were at least ten times greater than the filter blank average for most samples and elements, but all Ni measurements were less than six times greater than the blank. However, only two samples (Aer13 and Aer14) had blank-corrected Ni concentrations below the detection limit (calculated as 3σ of filter blank replicates).

Analysis of replicate filters from samples Aer03, Aer06, Aer09, and Aer12 demonstrated precision to be a function of both element and filter loading. Of these four samples, Aer06 had the highest concentrations for most elements and also most frequently showed the best precision for each element. Across all four sets of replicates, precision among replicates averaged 20–25% for most elements, but 35% for Ni

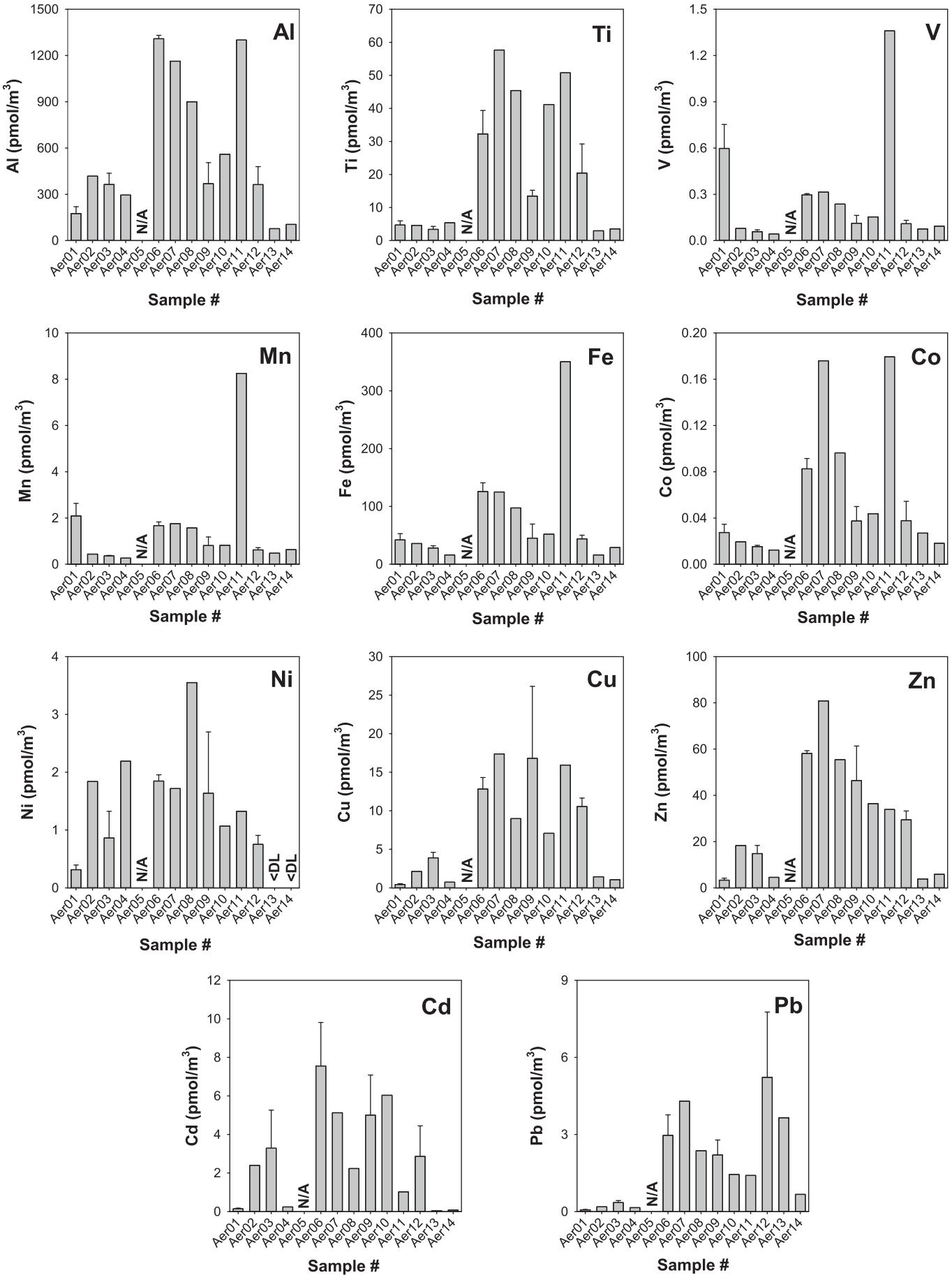

(caption on next page)

Fig. 2. Atmospheric concentrations (pmol m^{-3}) of selected elements for aerosol sample deployments during GN01. No data are shown for sample Aer05 (indicated by 'N/A'), due to the low volume of air sampled. ' < DL' indicates blank corrected concentrations less than three times the standard deviation of blank filter values. Error bars for samples Aer03, Aer06, Aer09, and Aer12 represent standard deviations of triplicate samples, while those for Aer01 represent uncertainty in the volume of air filtered.

Table 3
Mineral dust concentrations, in ng/m^3, measured in air masses over the Arctic Ocean and elsewhere, based on Al and Ti concentrations and average crustal Al and Ti content of 8.04% and 0.30% respectively (Taylor and McLennan, 1995). Values are given as a range, with median values in brackets.

Sampling location	Research cruise	Dust concentration from Al	Dust concentration from Ti	Reference
Arctic	GN01	26–439 (124)	47–920 (215)	This study
Arctic	ARK-XXVI/3	63–236 (112)[a]	157–1300 (227)[a]	(Kadko et al., 2016)
Arctic (open water)	IAOE-91	(97)	(90)	(Maenhaut et al., 1996)
Arctic (pack ice)	IAOE-91	(168)	(147)	(Maenhaut et al., 1996)
Equatorial Pacific	GP16	31–2558 (50)	137–3692 (255)	(Buck et al., this issue)[b]
North Atlantic	GA01	15–359 (166)	3–632 (209)	(Shelley et al., 2017)
N. Atlantic – marine	GA03	9–244 (38)	83–1062 (202)	(Shelley et al., 2015)
N. Atlantic – N. American	GA03	77–1105 (378)	455–2895 (869)	(Shelley et al., 2015)
N. Atlantic – European	GA03	818–1930 (1675)	921–3664 (2327)	(Shelley et al., 2015)
N. Atlantic – African	GA03	4233–93,097 (32,463)	9259–199,586 (68,320)	(Shelley et al., 2015)

[a] Three samples only.
[b] Data available at https://www.bco-dmo.org/dataset/675632/.

and 45% for Cd.

Both Al and Ti are commonly used as tracers of mineral dust in aerosol samples (Buck et al., 2010; Shelley et al., 2017) due to their relatively high abundance in crustal material (e.g. Taylor, 1964). This technique assumes that the Al (or Ti) is only associated with lithogenic aerosol material, rather than with sea salt mobilized from the sea surface or with aerosols originating from anthropogenic processes. Based on mean upper continental crust (UCC) Al and Ti content of 8.04% and 0.30% by mass, respectively (Taylor and McLennan, 1995), we calculate mineral dust loadings during GN01 of 26–439 ng m^{-3} using Al, or 47–920 ng m^{-3} using Ti. These values cover a range similar to dust loadings calculated from previous Arctic Ocean aerosol Al and Ti measurements (Table 3). They are also comparable to equatorial Pacific and North Atlantic samples with a "marine" provenance (i.e. samples for which air-mass back trajectories indicate no time spent over continental land masses during the three days before the air mass reached the sampling location) (Table 3). In contrast, the mineral aerosol loadings are approximately one and two orders of magnitude lower, respectively, than North Atlantic aerosols with European and African provenance collected during the US GEOTRACES GA03 study (Shelley et al., 2015) and in previous North Atlantic studies (Baker et al., 2006; Buck et al., 2010).

As with Al and Ti, aerosol concentrations of V, Mn, Fe, Co, and Ni during GN01 were similar to concentrations observed in the equatorial Pacific and North Atlantic in air masses with marine provenance and were lower than those in North Atlantic air masses that had travelled from Africa or Europe (Fig. 3; V not shown). However, median Fe, Mn, and Co concentrations during GN01 were approximately an order of magnitude lower than concentrations measured in three samples collected north of 80°N during the ARK-XXVI/3 study in August–September 2011 (Kadko et al., 2016). Median concentrations of Fe, Mn and V were also roughly an order of magnitude lower than late summer (August–October) average values in time-series (1980–2000) aerosol data from Alert, Canada (Gong and Barrie, 2005), though the latter data show significant spread. In contrast, the median GN01 Al and Ni concentrations were similar to their respective seasonal averages at Alert, and GN01 Ti concentrations were 3–4 times higher than the late summertime average for the Alert dataset, though again, the twenty year time series reveals a large range in measured concentrations during the August–October period.

Median aerosol concentrations of Cu, Zn, and Pb during GN01 were similar to concentrations reported for the high Arctic (> 80°N) during summertime (Kadko et al., 2016), and to their seasonal average concentrations in the Alert time-series (Gong and Barrie, 2005). They were generally higher than those measured in remote air masses, such as in the equatorial Pacific and in "marine-sourced" air masses in the North Atlantic during GEOTRACES cruises GA01 and GA03, and were closer to concentrations in North American influenced aerosols during the latter cruise (Fig. 4). However, they were still typically lower than concentrations measured in air masses of European and African (high dust) provenance during GA03. Higher concentrations associated with African-derived air masses during the latter are likely due to much higher loadings of mineral dust, whereas the high concentrations of these elements during GN01, as with the GA03 samples of North American and European provenance, most likely indicates transport of anthropogenic aerosols from industrial sources.

Concentrations of Cd during GN01 (0.04–7.55 pmol m^{-3}) were notable in that they reached the high end of concentrations documented for other regions (Fig. 4), although similarly high values have been previously reported for the Arctic region (up to 9 pmol m^{-3} at Spitsbergen (Pacyna and Ottar, 1985)). Despite these higher values, the lower end of the Cd, Cu, Zn and Pb concentration ranges measured during GN01 were close to values from the more remote air masses (Fig. 4). Together, these observations suggest that, although concentrations of these elements are not as significantly impacted by anthropogenic emissions as they are during the Arctic winter, the summertime Arctic air can still have a significant pollutant component relative to air masses in other remote regions.

Although the concentrations of some elements indicate anthropogenic contributions, air mass back trajectories do not reveal obvious recent transport from urban/industrial areas. For most deployments, the air sampled had spent little or no time over land in the three days before reaching the sampling area (Fig. S1). Samples with higher concentrations of many elements (Aer06-Aer08, Aer10, Aer11) tended to be associated with air masses moving towards the pole for at least some of the sampling period, though for Aer06-Aer08 this is in part due to the proximity of the sampling location to the North Pole and thus any air mass *must* have moved north to reach the area. In contrast, the samples with lower Al and Ti concentrations were typically associated with air mass back trajectories that indicate circumpolar or southward transport to reach the sampling area.

An alternative explanation for the observed distribution of certain aerosol TEs relates to findings during a previous shipboard study of summertime Arctic aerosols. Maenhaut et al. (1996) reported higher concentrations of lithogenic and anthropogenic elements in aerosol samples collected while in pack ice, relative to those collected in open

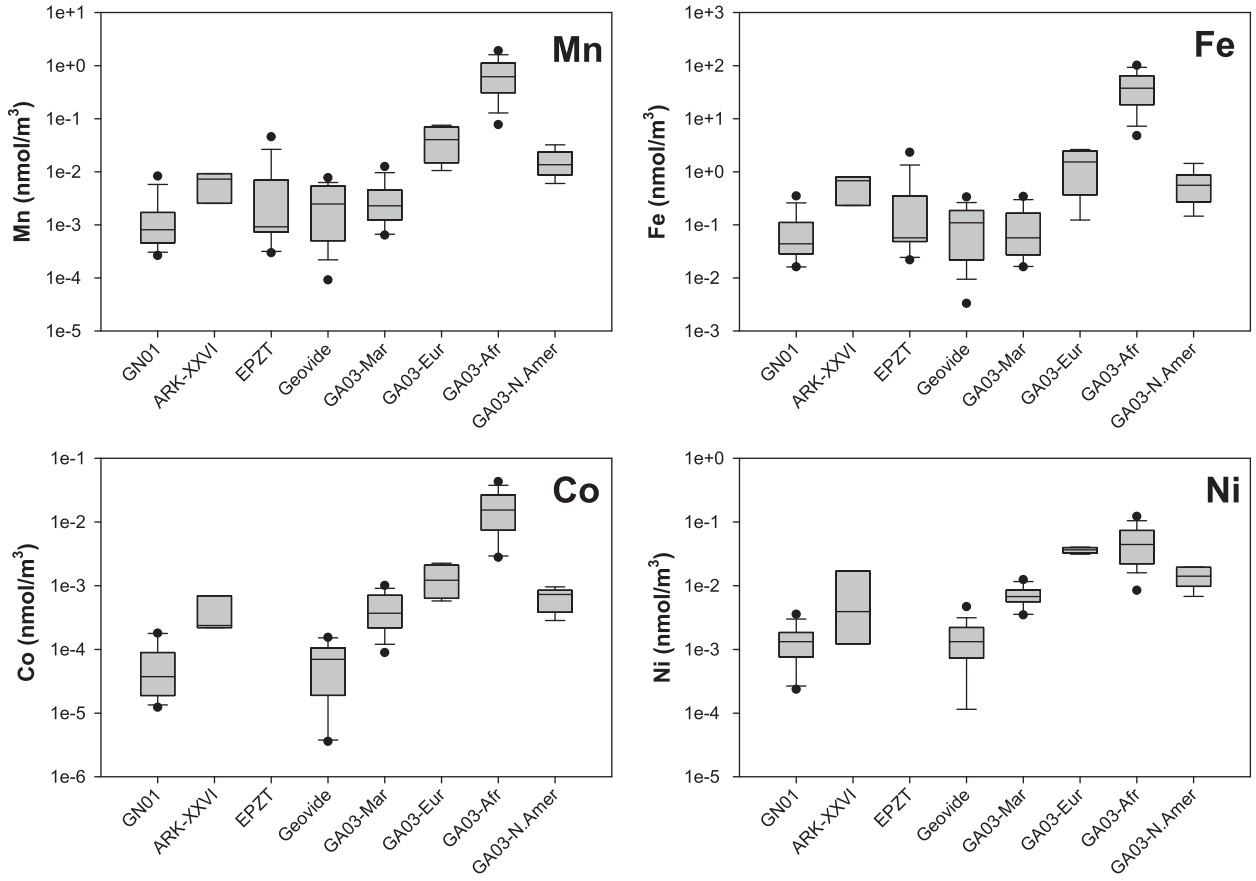

Fig. 3. Comparison of aerosol Mn, Fe, Co, and Ni concentrations during GN01 (at left) to those measured in previous studies in the Arctic (ARK-XXVI/3) (Kadko et al., 2016), equatorial Pacific (EPZT) (Buck et al., this issue), and North Atlantic (Geovides, GA03) (Shelley et al., 2017, 2015). GA03 data is split by provenance of air masses sampled (Eur. – European, Mar. – Marine, Afr. – African, N·Amer. – North American). Each dataset is shown as a box and whisker plot with the box covering the 25th–75th percentiles of data, the median shown by the horizontal line in the box, and whiskers spanning the 10th–90th percentiles of the dataset.

water. They suggested that this could be attributed to coarse aerosols being carried by wind blowing over the sea ice, mobilizing materials that had originated from Siberian river outflow and frozen into the ice. The spatial distribution of higher aerosol TE concentrations measured during GN01 could be a product of this process. Samples Aer12 to Aer14, which generally showed relatively low trace element concentrations, were collected south of 76.5°N, as the ship crossed open water, which is reflected in a relatively high sea-salt component to the aerosols collected (Mukherjee et al., 2017). The same is true for Aer01, collected while transiting northward over open water. Samples Aer02 to Aer04, which also had generally low TE loading, were collected within the marginal ice zone (Aer02) and in full sea ice coverage (Aer03 and Aer04), but in an area of relatively thin first year ice.

The samples with higher loading of mineral dust were collected while in more extensive sea ice (Aer06 to Aer10). For much of this time the ship was in a region potentially influenced by the Transpolar Drift, which transports both fluvial material and sediment-laden sea ice across the Arctic Ocean from the Siberian shelf seas (Klunder et al., 2012; Nürnberg et al., 1994). Indeed, the influence of the Transpolar Drift was evident from surface water data between Station 30, occupied 1st–3rd September on the northbound transect, to Station 43, occupied 15th–17th September on the southbound transect (unpublished data). The sea ice coverage at this time extended as far south as ~80°N (Fig. S2), and back-trajectories calculated for these aerosol samples indicate that the air masses sampled would have spent upwards of 12 h passing over sea ice before being sampled (Fig. S1). Thus, there may be a contribution to the higher aerosol loadings in this study from aerosols generated by surface winds blowing over sea ice, resulting either through erosion of material frozen into the ice or by resuspension of dust and/or snow previously deposited on top of the sea ice.

Concentrations of Fe, V, and Mn in Aer11 are notable in that they are at least 2–4 times higher than in any other sample, while Al, Ti, and Co in the same sample are among the highest measured during GN01 (Fig. 2). However, elevated concentrations are not seen for Ni, Zn, Cd or Pb. HYSPLIT back trajectories suggest that the start of sampling for Aer11 coincided with influence from an air mass moving northward from mainland Canada, while the latter part of the deployment may have been influenced by a Siberian source (Fig. S1). Therefore the relatively high concentrations of these elements may reflect a significant contribution from lithogenic aerosol material in Aer11 due to its recent transport from a continental area.

3.2. Elemental ratios and enrichment factors

Both Al and Ti are frequently used as tracers of crustal material in aerosol samples, and comparison of the TE/Al or TE/Ti ratios in aerosol samples to those typical of crustal material can inform about the non-crustal contributions of those TEs (Chester et al., 1993; Peirson et al., 1974). In doing so, one must consider the caveat that elemental composition (and therefore elemental ratios) of source minerals can vary quite significantly from average crustal values. For example, the Ti/Al ratios of aerosol and soil samples reported from different areas within the North Africa region vary by at least a factor of four (Gelado-Caballero et al., 2012). In using either Al or Ti as a mineral dust tracer, it is also assumed that there is a negligible contribution from anthropogenic or sea-salt sources.

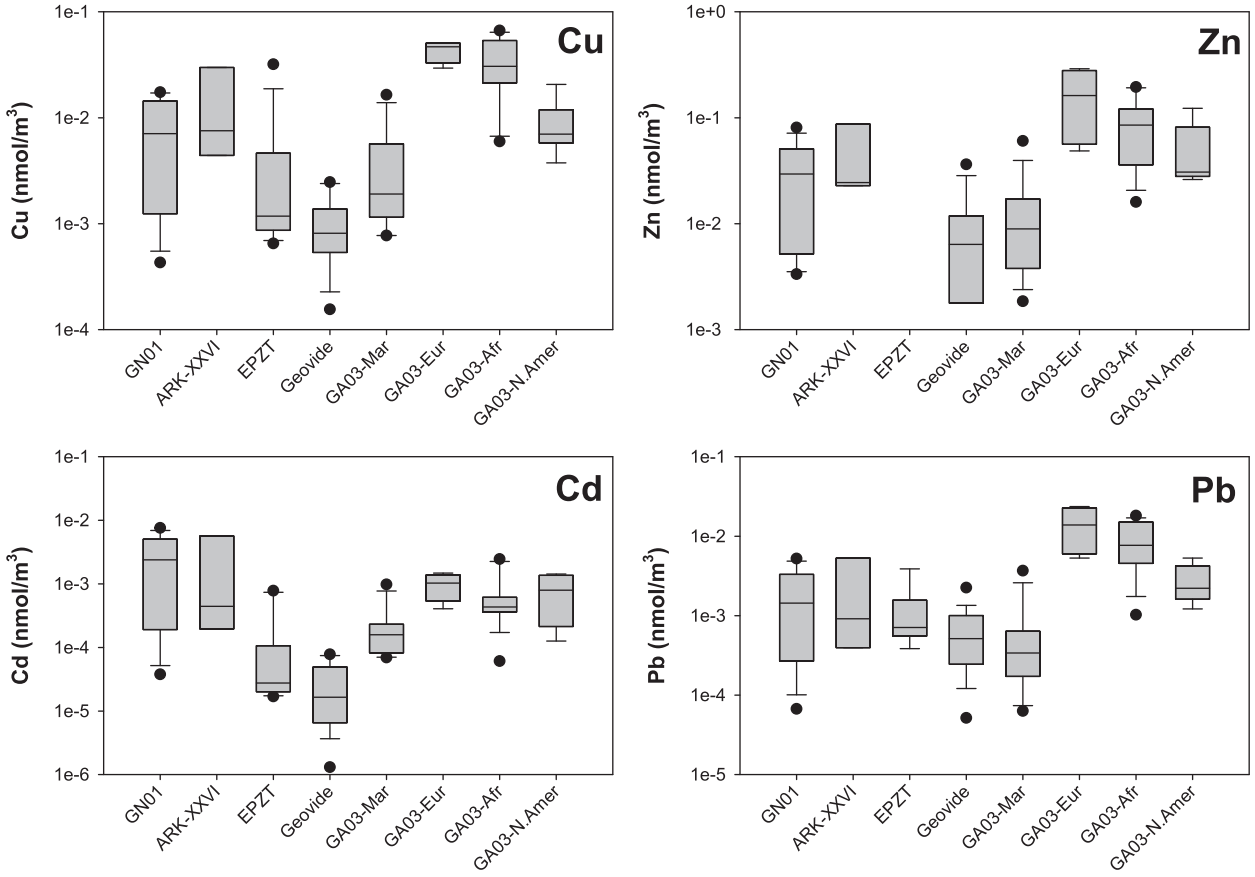

Fig. 4. Comparison of aerosol Cu, Zn, Cd, and Pb concentrations during GN01 (at left) to those measured in previous studies in the Arctic and elsewhere (names as in caption for Fig. 3). Each dataset is shown as a box and whisker plot with the box covering the 25th–75th percentiles of data, the median shown by the horizontal line in the box, and whiskers spanning the 10th–90th percentiles of the dataset.

The Ti/Al, Fe/Al and Fe/Ti molar ratios for all GN01 aerosol samples except Aer05 are presented in Fig. 5. For Ti/Al, the values fall either side of the UCC average (Fig. 5a), with Ti/Al values for Aer02 to Aer04 as low as 40% of the UCC average, while the remaining samples have a Ti/Al of up to 3.5 times the average crustal ratio. The variability in Ti/Al is similar to that observed in a series of twelve daily samples collected at Alert during springtime, which ranged from 0.01–0.37 mol mol^{-1}, despite the concentrations of both elements following similar trends over the study period (Landsberger et al., 1990). Most Fe/Al values, excluding samples Aer01, Aer11, and Aer14, fall below the average UCC value, as do all Fe/Ti values (Fig. 5b and c). While these relatively low ratios could potentially indicate additional, non-mineral dust contributions to aerosol Al and Ti, the low dust concentrations observed during this study, along with the fact that Ti/Al ratios are close to crustal values, suggests that the low Fe/Ti and Fe/Al ratios instead represent a crustal source that is relatively depleted in Fe. Again, the observed deviations from average crustal ratios are not unusual, falling at the low end of the Fe/Ti range (2.4–333 mol mol^{-1}) reported over a 12-day period in the Canadian Arctic by Landsberger et al. (1990), and similar to the range reported along a meridional transect of the North Atlantic (Buck et al., 2010).

A similar pattern of TE/Al (and TE/Ti) ratios lower than average crustal values was seen in the GN01 aerosol data for V, Mn, and Co. In contrast, Ni, Cu, Zn, Cd and Pb in each aerosol sample were enriched over Al, relative to UCC values. The increased concentrations of different elements in aerosol samples, relative to a specified source material, is often described in terms of an enrichment factor, EF (Peirson et al., 1974). To compare samples to crustal material, the EF can be calculated as follows:

$$EF = (TE/Al)_{sample}/(TE/Al)_{crust} \quad (1)$$

where $(TE/Al)_{sample}$ is the trace element to Al ratio in the sample and $(TE/Al)_{crust}$ is the average crustal element to Al ratio. The TE/Ti ratio can also be used for crustal material, but we compare to Al data here because of higher sample Al concentrations relative to filter blanks. Due to the variability in crustal elemental ratios, EF values of < 10 are generally not considered to reflect significant enrichments in an element relative to crustal material, while values > 10 are considered to be significantly enriched (e.g. Chester et al., 1993). In this case we calculated EF values for Ti, V, Mn, Fe, Co, Ni, Cu, Zn, Cd, and Pb using average UCC TE/Al values from Taylor and McLennan (1995). The resulting distributions of EF values (Fig. 6) look very similar if average crustal TE/Ti values are used instead (data not shown).

Fig. 6 illustrates that none of the GN01 aerosol samples were significantly enriched in Ti, V, Mn, Fe, or Co over Al, relative to average crustal material. This is unsurprising for Ti and Fe, both of which have relatively high concentrations in lithogenic material and are typically dominated by a natural mineral dust contribution in aerosols (e.g. Buck et al., 2013; Shelley et al., 2015). Although Fe is enriched in some anthropogenic emissions, such as from industrial coal combustion and the combustion products of heavy fuel oil (Desboeufs et al., 2005; Luo et al., 2008), the prevalence of mineral dust and its relatively high Fe content means that even at some urban sites, aerosol Fe exhibits no significant enrichment over crustal material (Chester et al., 2000). Previous aerosol measurements from the Arctic also indicate strong coupling between Fe, Al, and Ti concentrations. Kadko et al. (2016) found EFs of 0.18–0.49 for Al and 1–7 for Fe (based on TE/Ti ratios) in three samples from the high Arctic during summer 2011, and statistical analysis of the 21 year time-series dataset from Alert grouped the three

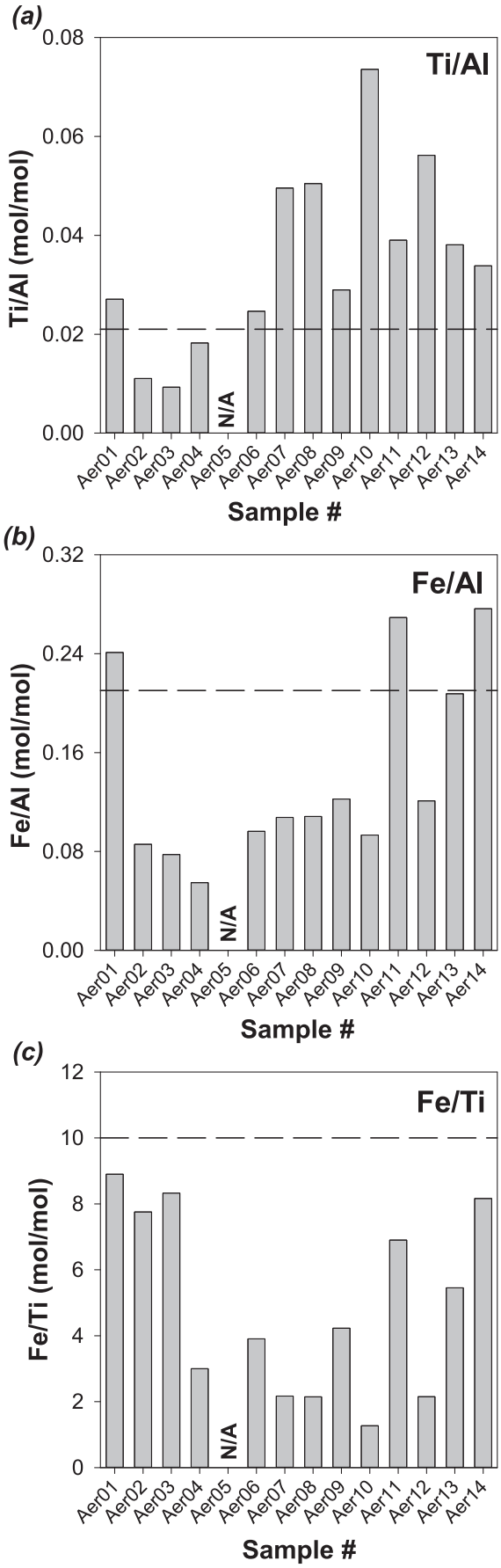

Fig. 5. Molar ratios of Al, Ti and Fe for all GN01 samples except sample Aer05 (due to low air volume sampled): (a) Ti/Al, (b) Fe/Al, (c) Fe/Ti. Dashed horizontal line in each plot represents the upper continental crust molar ratio (Taylor and McLennan, 1995).

elements together as mainly soil influenced (Gong and Barrie, 2005).

The lack of V, Mn, and Co enrichments are also not unexpected, though each is sometimes found to be enriched in aerosols sampled elsewhere (e.g. Chance et al., 2015; Shelley et al., 2017, 2015). Aerosol concentrations of V are sometimes enriched over crustal values due to contributions from the combustion products of crude oil (Chen and Duce, 1983), while enrichments in Co and Mn have been attributed to release during smelting and from the use of Mn as an additive in vehicle fuels (Fomba et al., 2013; Laing et al., 2014b; Wallace and Slonecker, 1997). However, aerosol V, Mn, and Co concentrations also often follow those of crustal elements, with EF < 10 often reported, including in some "urban-rich" aerosols (Chester et al., 2000, 1993; Shelley et al., 2017).

In Arctic aerosol datasets, Kadko et al. (2016) calculated EF values for V, Mn, and Co of < 10, with those for V being < 1 (i.e. aerosols had V/Ti ratios lower than that of the crustal reference value used), as was generally the case in this study. Gong and Barrie (2005) found variations in aerosol Mn concentrations at Alert to generally follow those of Fe and Al, while V concentrations showed strong seasonal variations more typical of anthropogenic elements. However, "non-soil" fractions of V and Mn, calculated by subtracting the lithogenic contribution based on ratios to Al, and often used as proxies of anthropogenic contributions to V and Mn (Sirois and Barrie, 1999; Zhan et al., 2014), each showed minima in concentrations during the summer months in the Alert dataset (Sirois and Barrie, 1999), and the low EFs for Mn and V in our own data suggest no significant non-soil contributions for this time of year.

Enrichment factors for Ni in GN01 samples ranged from 9 to 65, based on Ni/Al ratios, while all Cu, Zn, Cd and Pb EFs were > 10 (Fig. 6). This is typical for aerosols collected in various other regions, with the exception of those heavily influenced by mineral dust (Buck et al., 2013; Chester et al., 2000; Patey et al., 2015; Shelley et al., 2017, 2015), and is consistent with the anthropogenic enrichment of these elements in Arctic aerosols observed in previous studies (Gong and Barrie, 2005; Kadko et al., 2016; Shevchenko et al., 2003; Zhan et al., 2014). Anthropogenic sources of these elements include coal and oil combustion in power stations, roasting and smelting of non-ferrous metal ores, refuse incineration, gasoline combustion, and cement production (Pacyna and Pacyna, 2001). Combustion of heavy fuel oils, including marine fuel oils, is a major source of Ni, as well as V, to the extent that the two are used as markers for shipping emissions (Celo et al., 2015; Streibel et al., 2017). However, the V/Ni ratios measured in this study (0.02–1.9 mol mol^{-1}) were generally significantly lower than both the range typical of shipping emissions (2.3–5.8 mol mol^{-1}) (Celo et al., 2015; Viana et al., 2009) and the average crustal value (3.5 mol mol^{-1}) (Taylor and McLennan, 1995), suggesting a different Ni source and negligible influence from heavy fuel oil combustion on the aerosols sampled. Although fuel oil combustion is considered to be by far the main anthropogenic source of aerosol Ni on a global basis (Pacyna and Pacyna, 2001), several studies from the Eurasian Arctic indicate that emissions from non-ferrous metal smelters in northern Eurasia represent the most significant local anthropogenic contribution to aerosol Ni, as well as being important sources of aerosol Cu, Zn, Cd and Pb (Berg et al., 2008; Laing et al., 2014a, 2014b; Shevchenko et al., 2003).

Enrichment factors for Cu, Zn and Pb were somewhat higher than those calculated from three high Arctic aerosol samples collected during summer 2011 (Kadko et al., 2016) and of a similar magnitude to the "European" influenced North Atlantic samples reported by Shelley et al. (2015). However, the Cd EF values calculated for GN01 samples

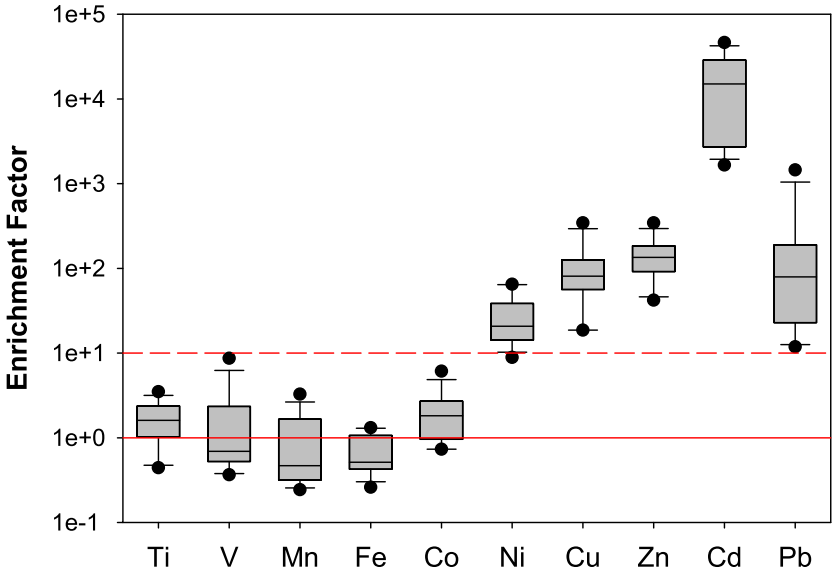

Fig. 6. Enrichment factors for different trace elements in GN01 aerosols, relative to Al in upper continental crust (UCC) material (Taylor and McLennan, 1995). Box plots show the 25th–75th percentiles of the data as the box, bisected by the median. Whiskers show the range of the 10th–90th percentiles of the data, with outliers marked by black dots. The solid horizontal line indicates an EF of 1 (i.e. TE/Al ratio equal to that of UCC) and the dashed horizontal line indicates an EF of 10 (EF > 10 indicates significant enrichment).

were up to an order of magnitude greater than those reported during ARK-XXVI/3 (Kadko et al., 2016), due to generally higher Cd concentrations during GN01. Cadmium EF values for GN01 were also significantly higher than any reported from recent GEOTRACES studies in the North Atlantic and equatorial Pacific Oceans. Again, this is primarily due to higher Cd concentrations measured during GN01 (Fig. 4).

Table 4 shows a matrix of Spearman Rank Order correlation coefficients (ρ) for the TE concentrations we observed, based on thirteen aerosol samples from GN01 (Aer05 was excluded due to the low sample volume). It indicates strong correlations (ρ > 0.7) between Al and the non-enriched elements, Ti, Fe, and Co, but also strong correlations between Al and Cu, Zn, and Cd. This could indicate that much of the aerosol Cu, Zn and Cd is of lithogenic origin, and that the observed EFs are due to a natural dust source that is relatively enriched in these elements (and depleted in Mn and Fe), relative to average UCC material. Alternatively, the correlations could simply reflect that samples with a higher aerosol load included higher loadings of both natural dust and anthropogenic aerosols. In contrast, V and Mn show only moderate correlations with Al. This is not due to anthropogenic enrichment of aerosol V and Mn, as each had EFs of < 10 in all samples (and often < 1). Table 4 also shows that aerosol Ni and Pb concentrations had weak to moderate correlations with the other TEs. This may indicate that the sources of these two elements are distinct from the other TEs and from each other.

3.3. Trace element atmospheric deposition estimates

In many remote ocean regions, atmospheric deposition is considered to be a major source of ecologically important TEs to surface waters, and the supply rate of aerosol iron, in particular, can influence rates of primary productivity (Jickells et al., 2005; Moore et al., 2004). This is unlikely to be the case in the Arctic Ocean, where Eurasian river inputs have a significant influence on some TE distributions (Klunder et al., 2012; Middag et al., 2011). However, the Arctic Ocean remains a region that is under-sampled with respect to in situ observations of atmospheric deposition, which limits our ability to verify the accuracy of global atmospheric deposition models (e.g. Mahowald et al., 2009). In addition, with the Arctic climate changing rapidly, understanding the relative magnitude of micronutrient and pollutant TE inputs from different sources can help us predict how Arctic biogeochemistry may be affected in the coming decades (Macdonald et al., 2005).

Aerosol TE concentrations (C) are often used to calculate dry deposition flux (F_{dry}) through the equation:

$$F_{dry} = C \times V_{dry} \quad (2)$$

where V_{dry} is the dry deposition velocity (Duce et al., 1991). However, V_{dry} is sensitive to particle size, as well as wind speed, relative humidity and other factors, and parameterizations of F_{dry} are often simplified by using fixed values of V_{dry}, with the caveat that there is considerable uncertainty associated with the chosen velocity (Buck et al., 2010; Chance et al., 2015; Duce et al., 1991), leading to uncertainties in dry deposition of up to an order of magnitude.

Here we instead calculate a value for the bulk (i.e. dry and wet) atmospheric deposition velocity, using ^{7}Be atmospheric aerosol data and the ^{7}Be inventory associated with recent snowfall, employing an approach similar to that used previously (Kadko et al., 2016, 2015). We

Table 4
Matrix of Spearman Rank Order correlation coefficients (ρ) for the reported TEs, based on all samples except Aer05 (due to low volume of air sampled). Values of ρ > 0.7 are in bold. Correlations significant at the $p < 0.01$ level are italicized.

	Al	Ti	V	Mn	Fe	Co	Ni	Cu	Zn	Cd
Ti	***0.802***									
V	0.593	***0.725***								
Mn	0.538	*0.681*	***0.989***							
Fe	***0.885***	***0.896***	***0.857***	***0.819***						
Co	***0.758***	***0.874***	***0.852***	***0.830***	***0.923***					
Ni	0.643	0.500	0.060	0.017	0.396	0.220				
Cu	***0.753***	***0.714***	0.484	0.445	***0.769***	***0.758***	0.319			
Zn	***0.863***	***0.791***	0.484	0.445	***0.819***	***0.747***	0.588	***0.885***		
Cd	***0.720***	0.522	0.253	0.187	0.582	0.423	0.396	*0.687*	***0.791***	
Pb	0.280	0.401	0.198	0.198	0.379	0.577	−0.044	0.670	0.588	0.363

then provide estimates for dry deposition of TEs by combining our bulk atmospheric flux values with data from the literature.

The short-lived radioisotope, ^{7}Be, is formed in the atmosphere by gas-phase nuclear transformations and quickly attaches to aerosol particles, prior to wet and dry deposition with those particles. It has been shown (Kadko et al., 2015) that the bulk deposition flux of a trace element (F_{TE}) can be related to that of ^{7}Be (F_{7Be}, derived from the measured inventory) by:

$$F_{TE} = F_{7Be} \times \left[\frac{C_{TE}}{C_{7Be}}\right] \quad (3)$$

where $[C_{TE}/C_{7Be}]$ is the ratio of a trace element to ^{7}Be measured on aerosols. Formulated in another way, the ratio F_{7Be}/C_{7Be} can be considered as an effective bulk deposition velocity, V_{bulk}, such that:

$$F_{TE} = V_{bulk} \times C_{TE} \quad (4)$$

This method was applied to waters off Bermuda and shown to give comparable results to wet plus dry TE fluxes independently measured on the island (Kadko et al., 2015). The inter-seasonal variability of the aerosol ^{7}Be activity over Bermuda is only about a factor of 2–3 (Arimoto et al., 1999; Kadko et al., 2015) with the consequence that the cumulative ^{7}Be ocean inventory, from progressive input and decay of the input flux, does not vary by greater than 20% throughout the year (Kadko et al., 2015; Kadko and Prospero, 2011). Therefore, the ocean inventory measured at any one time is representative (to within 20%) of the instantaneous ^{7}Be flux. In the Arctic, the situation is more complicated, as the aerosol ^{7}Be activity exhibits significant seasonal variability (Dibb et al., 1994; Kadko et al., 2016). For that reason, the measurement of the system inventory at one time cannot reflect the instantaneous flux, but rather an integration of the flux over the previous 77 d mean life of ^{7}Be. Previously, Kadko et al. (2016) modeled the seasonal variation of aerosol ^{7}Be concentration and the flux to the Arctic and derived a bulk deposition velocity of 1350 m d^{-1}.

Here, a somewhat different approach is used. The GN01 timeframe overlapped with the end of summertime melting and the start of fresh snow accumulation on the sea ice, which allowed samples of freshly fallen snow to be collected for ^{7}Be analysis at six ice stations (Table 2a). From the resulting ^{7}Be activity measurements and the date of sample collection, instantaneous values of ^{7}Be flux (dpm m^{-2} d^{-1}) were estimated using:

$$F_{7Be} = \lambda \bullet A_s/(1 - exp(-t \bullet \lambda)) \quad (5)$$

This equation is derived from the radioactivity ingrowth equation for a constant production rate, with the ^{7}Be deposition flux representing the production rate, λ is the ^{7}Be decay constant (0.013 d^{-1}), A_s is the activity of ^{7}Be measured per m^2 in the collected snow, and t is the time between onset of snowfall and sample collection date. Initial observations of snowfall were recorded on August 23rd. The results for F_{7Be} are shown in Table 2a. Flux determinations were also made from buckets deployed near the aerosol collectors, each of which collected a mixture of dry deposition and snowfall from events that ranged from brief flurries to hours-long events. Eq. (5) was likewise applied to the ^{7}Be activity measured in these bucket samples to calculate F_{7Be} (Table 2b).

Table 5
Aerosol ^{7}Be activity from six samples, along with the mean (± 1 SD) value.

Sample	^{7}Be (dpm m^{-3})
Aer04	0.044 ± 0.033
Aer06	0.023 ± 0.012
Aer07	0.036 ± 0.029
Aer09	0.028 ± 0.019
Aer10	0.042 ± 0.009
Aer11	0.034 ± 0.008
Mean ± 1SD	**0.034 ± 0.008**

In addition, replicate filters from aerosol samples Aer04, Aer06, Aer07, Aer09, Aer10 and Aer11 were analyzed for ^{7}Be. Data from these are shown in Table 5. Using this aerosol ^{7}Be concentration data (C_{7Be}; dpm m^{-3}) with the F_{7Be} flux measurements, the bulk deposition velocity can be derived as:

$$V_{bulk} = \frac{F_{7Be}}{C_{7Be}} \quad (6)$$

Implicit in this approach is the assumption that the sum of dry and wet deposition rates of ^{7}Be-bearing aerosols is approximately equal to that of the TE of interest, driven by a balance of dry deposition velocity and scavenging ratio for different size particles (Kadko et al., 2015; Shelley et al., 2017). Applying the average aerosol ^{7}Be from Table 5 (0.034 ± 0.008 dpm m^{-3}) and the average ^{7}Be flux from Table 2a (33.3 ± 10.8 dpm m^{-2} d^{-1}) to Eq. (6) we calculate a bulk deposition velocity of 970 ± 390 m d^{-1}, while using the alternative flux value from the bucket samples (44.9 ± 29.0 dpm m^{-2} d^{-1}; Table 2b) gives a V_{bulk} of 1310 ± 900 m d^{-1}. Both values are comparable to the value of 1350 m d^{-1} derived by modeling the seasonal variability of the Arctic Ocean inventory (Kadko et al., 2016) and fall within the range of bulk deposition velocities calculated using a ^{7}Be approach during a North Atlantic study (610–2800 m d^{-1}) (Shelley et al., 2017).

Taking the average of our two estimates of the bulk deposition velocity gives a V_{bulk} value of 1140 ± 490 m d^{-1}, which we apply to our aerosol TE concentrations to estimate the bulk depositional flux using Eq. (4) (Fig. 7a, Table 6). By extrapolating the daily Al deposition flux, and using 8% by mass average Al content of lithogenic material (Taylor and McLennan, 1995), we calculate a range of values for the annual dust flux to the Arctic Ocean of 11–182 mg m^{-2} y^{-1}, with a median value of 52 mg m^{-2} y^{-1} (Fig. 7b), which agrees with modeled dust fluxes to the Arctic region of < 200 mg m^{-2} y^{-1} (Jickells et al., 2005). Similarly, extrapolating our calculated Fe bulk deposition flux to an annual estimate gives a median atmospheric Fe flux of 1.0 mg m^{-2} y^{-1}; slightly lower than the modeled atmospheric Fe deposition to the Arctic region of 2–10 mg m^{-2} y^{-1} (Mahowald et al., 2009).

We note that extrapolating our summertime aerosol data to calculate annual deposition flux could over- or under-estimate annual atmospheric deposition if there are seasonal changes in the aerosol concentrations or the bulk deposition velocity. Time series data from the Canadian Arctic indicate only minor seasonality in aerosol Al and Fe concentrations, though the variations in some other elements are much greater (Gong and Barrie, 2005). Seasonal changes in the bulk deposition velocity are also possible, arising from variations in the relative importance of dry versus wet deposition, and from seasonal shifts in particle size distribution due to changes in transport pathways, photochemistry, and the influence of open water on contributions from sea-salt particles (Sirois and Barrie, 1999; Tunved et al., 2013).

Our bulk deposition velocity calculated from ^{7}Be data is close to the 1000 m d^{-1} often applied to calculate *dry* deposition associated with particles of > 1 μm, or alternatively applied to elements with low EFs (i.e. "crustal" elements) (Buck et al., 2010, 2006; Shelley et al., 2017). However, it is significantly greater than the 86–260 m d^{-1} (0.1–0.3 cm s^{-1}) values often applied to calculate dry deposition of fine (< 1 μm) aerosol particles or aerosols considered to be highly influenced by anthropogenic contributions from high-temperature combustion (Baker et al., 2007, 2003; Chance et al., 2015; Shelley et al., 2017). In addition, in locations such as the Arctic Ocean that are distant from major dust sources, it may be expected that the average particle size would be smaller, through settling and scavenging of particles during extended transport from source regions, resulting in a lower average dry deposition velocity for the remaining, smaller particles. Indeed, Davidson et al. (1985) calculated a dry deposition velocity for Al to the Greenland Ice Sheet of 0.2 cm s^{-1} (~170 m d^{-1}).

Applying commonly used dry deposition velocities of 1000 m d^{-1} and 260 m d^{-1} to GN01 aerosol TE concentrations would suggest that the dry deposition flux accounts for 88% and 23% of the calculated bulk

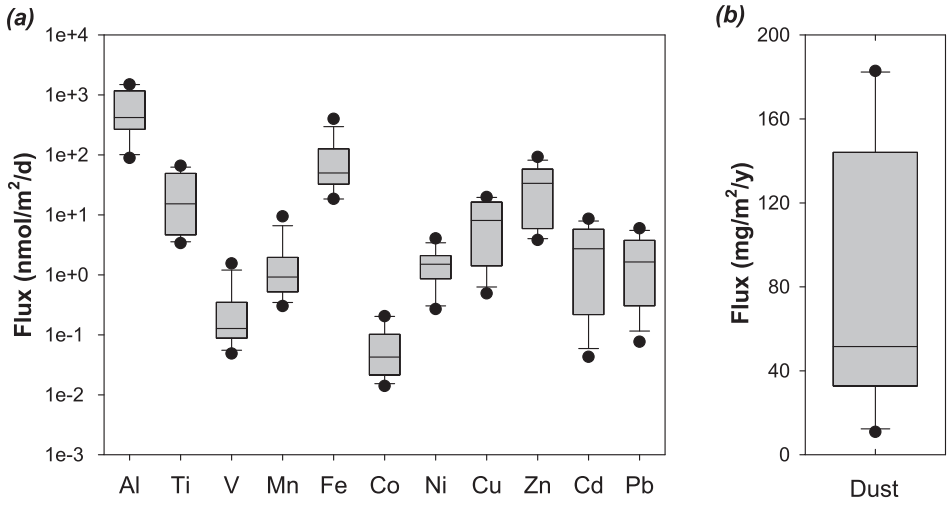

Fig. 7. Box plots showing bulk deposition fluxes calculated by applying the ^{7}Be-derived deposition velocity of 1140 m d^{-1} and GN01 aerosol TE concentrations to Eq. (4). (a) Daily deposition fluxes calculated for selected trace elements during GN01. (b) Range and median annual dust deposition flux to the Arctic Ocean, calculated by extrapolating the daily Al flux and assuming 8% Al by mass in mineral dust.

Table 6
Estimates of trace element dry deposition flux, given as ranges based on aerosol concentrations measured during GN01 and using 5% and 40% dry deposition contributions to bulk deposition to calculate V_{dry} values of 57 m d^{-1} and 456 m d^{-1}, respectively. Also given for comparison is the range of bulk deposition flux for each TE, as shown in Fig. 7.

	Range of dry deposition fluxes (nmol m^{-2} d^{-1})[a]		Bulk deposition flux (nmol m^{-2} d^{-1})[b]
	(V_{dry} = 57 m d^{-1})	(V_{dry} = 456 m d^{-1})	
Al	4.4–74.6	35–597	89–1492
Ti	0.17–3.3	1.3–26.3	3.4–65.7
V	0.002–0.078	0.02–0.62	0.05–1.55
Mn	0.015–0.470	0.12–3.76	0.30–9.41
Fe	0.92–19.97	7.4–159.7	18–399
Co	0.001–0.010	0.01–0.08	0.01–0.20
Ni	0.01–0.20	0.11–1.62	0.27–4.05
Cu	0.02–0.99	0.20–7.92	0.49–19.8
Zn	0.19–4.61	1.5–36.8	3.8–92
Cd	0.002–0.43	0.02–3.44	0.04–8.61
Pb	0.004–0.298	0.03–2.38	0.08–5.96

[a] Flux ranges calculated by applying Eq. (2), using minimum and maximum aerosol TE concentrations and stated dry deposition velocities.

[b] Calculated using Eq. (4) and a bulk deposition velocity of 1140 m d^{-1}.

deposition flux, respectively. There have been few studies of the relative magnitude of dry and wet deposition of TEs in the Arctic. Rahn (1981) estimated that for submicron aerosol particles at Barrow, Alaska, dry deposition should contribute only 5% of total deposition, though large uncertainties in the assumptions made were acknowledged. Davidson et al. (1981) calculated dry deposition to contribute < 25% of total annual deposition for enriched elements to the Greenland Ice Sheet, while suggesting that the number may be higher for crustal elements. On a global basis, Duce et al. (1991) calculated dry deposition to account for 40% of mineral aerosol and 17% of anthropogenic aerosol deposition to the oceans.

Based on the dominance of the wet deposition contribution in these previous estimates, it seems likely that the bulk TE deposition fluxes calculated here are strongly influenced by a wet deposition contribution from snowfall (i.e. the calculated deposition velocity is heavily influenced by a wet deposition contribution). In Table 6, we apply the minimum and maximum dry deposition contributions from these literature estimates (5% and 40%) to our bulk deposition fluxes and calculate in each case a range of dry deposition flux (F_{dry}) values for each TE for the summertime Arctic Ocean. In doing so, we also derive a range of potential dry deposition velocities (V_{dry}) by substituting the calculated F_{dry} values into Eq. (2). This gives V_{dry} values of 57 m d^{-1} (0.07 cm s^{-1}) or 456 m d^{-1} (0.5 cm s^{-1}), based on 5% or 40% contributions from dry deposition to bulk atmospheric deposition.

The GN01 research cruise coincided with the seasonal minimum in Arctic sea ice extent in September (Comiso, 2012). The calculated bulk deposition fluxes of TEs summarized in Fig. 7 therefore represent deposition that takes place when the amount of open water in the Arctic Ocean is at its greatest, and can be used to calculate the magnitude of summertime direct atmospheric input of TEs to the surface ocean in building TE budgets for the region. The current trend of a warming Arctic climate and more extensive sea ice melting during the summer months will act to increase this direct atmospheric contribution to the surface ocean inventory over time. However, this effect may be counterbalanced or exacerbated by other effects that result from a changing Arctic climate. These may include: changes in dust sources and/or frequency of forest fires brought about by changes in precipitation patterns further south; changes in mining and transportation activities within and adjacent to the Arctic region; changes to air mass transport to the Arctic resulting from a reduction in temperature gradient between the Arctic and mid-latitude areas; and changes in precipitation patterns over the Arctic Ocean itself.

4. Conclusions

The Arctic Ocean is a region characterized by significant seasonality in aerosol concentrations, with much previous research focused on the accumulation of atmospheric pollutants during the winter months. Our samples, collected late in the summer of 2015, reveal relatively low concentrations of mineral dust aerosols and low concentrations of the key micronutrient Fe, consistent with air mass back trajectory analyses that suggest no recent transport from major dust sources. However, concentrations of some TEs in our samples, notably Cd, Pb, Cu and Zn, showed significant enrichments over typical crustal material, apparently indicating an anthropogenic component that may have remained in the atmosphere longer due to smaller particle size, though this cannot be verified from the current data.

Using ^{7}Be flux data (from freshly fallen snow) and ^{7}Be activity of aerosol samples, we calculated a bulk depositional velocity of 1140 ± 490 m d^{-1}, which was used along with aerosol TE concentration data to estimate bulk deposition fluxes of the trace elements of interest to the Arctic region during the summer months. Our calculated bulk deposition fluxes of mineral dust and aerosol Fe, along with literature estimates of the dry deposition percentage contribution to bulk deposition, highlight the low rates of dust deposition and atmospheric Fe supply to the central Arctic during the summer months.

Acknowledgements

This research was supported by National Science Foundation awards OCE-1438047 to CSB, OCE-1434085 to DK, OCE-1437266 to WML, and OCE-1436019 to PLM, as well as OCE-1355913. A portion of this work was performed at the National High Magnetic Field Laboratory, which is supported by NSF Cooperative Agreement # DMR-1157490 and the State of Florida. The authors gratefully acknowledge Dr. Neil Wyatt, Dr. Mark Stephens, Paul Aguilar and Bill Schmoker for their shipboard assistance, and the officers and crew of the USCGC *Healy* for their support during US GEOTRACES GN01.

Appendix A. Supplementary material

Supplementary material to this article can be found online at https://doi.org/10.1016/j.chemgeo.2018.06.007.

References

Arimoto, R., Duce, R.A., Ray, B.J., Ellis Jr., W.G., Cullen, J.D., Merrill, J.T., 1995. Trace elements in the atmosphere over the North Atlantic. J. Geophys. Res. Atmos. 100, 1199–1213. http://dx.doi.org/10.1029/94JD02618.

Arimoto, R., Snow, J.A., Graustein, W.C., Moody, J.L., Ray, B.J., Duce, R.A., Turekian, K.K., Maring, H.B., 1999. Influences of atmospheric transport pathways on radionuclide activities in aerosol particles from over the North Atlantic. J. Geophys. Res. Atmos. 104, 21,301–21,316. http://dx.doi.org/10.1029/1999JD900356.

Arimoto, R., Duce, R.A., Ray, B.J., Tomza, U., 2003. Dry deposition of trace elements to the western North Atlantic. Glob. Biogeochem. Cycles 17, 1010. http://dx.doi.org/10.1029/2001GB001406.

Armstrong, R.A., Lee, C., Hedges, J.I., Honjo, S., Wakeham, S.G., 2002. A new, mechanistic model for organic carbon fluxes in the ocean based on the quantitative association of POC with ballast minerals. Deep-Sea Res. II Top. Stud. Oceanogr. 49, 219–236. http://dx.doi.org/10.1016/S0967-0645(01)00101-1.

Baker, A.R., Kelly, S.D., Biswas, K.F., Witt, M., Jickells, T.D., 2003. Atmospheric deposition of nutrients to the Atlantic Ocean. Geophys. Res. Lett. 30, 2296. http://dx.doi.org/10.1029/2003GL018518.

Baker, A.R., Jickells, T.D., Witt, M., Linge, K.L., 2006. Trends in the solubility of iron, aluminium, manganese and phosphorus in aerosol collected over the Atlantic Ocean. Mar. Chem. 98, 43–58. http://dx.doi.org/10.1016/j.marchem.2005.06.004.

Baker, A.R., Weston, K., Kelly, S.D., Voss, M., Streu, P., Cape, J.N., 2007. Dry and wet deposition of nutrients from the tropical Atlantic atmosphere: links to primary productivity and nitrogen fixation. Deep-Sea Res. I Oceanogr. Res. Pap. 54, 1704–1720. http://dx.doi.org/10.1016/j.dsr.2007.07.001.

Barrie, L.A., 1986. Arctic air chemistry: an overview. In: Stonehouse, B. (Ed.), Arctic Air Pollution. Cambridge University Press, Cambridge, UK, pp. 5–23.

Barrie, L.A., Hoff, R.M., 1985. Five years of air chemistry observations in the Canadian Arctic. Atmos. Environ. 19, 1995–2010. http://dx.doi.org/10.1016/0004-6981(85)90108-8.

Berg, T., Aas, W., Pacyna, J., Uggerud, H.T., Vadset, M., 2008. Atmospheric trace metal concentrations at Norwegian background sites during 25 years and its relation to European emissions. Atmos. Environ. 42, 7494–7501. http://dx.doi.org/10.1016/j.atmosenv.2008.05.020.

Boyd, P.W., Ibisanmi, E., Sander, S.G., Hunter, K.A., Jackson, G.A., 2010. Remineralization of upper ocean particles: implications for iron biogeochemistry. Limnol. Oceanogr. 55, 1271–1288. http://dx.doi.org/10.4319/lo.2010.55.3.1271.

Buck, C.S., Landing, W.M., Resing, J.A., Lebon, G.T., 2006. Aerosol iron and aluminum solubility in the northwest Pacific Ocean: results from the 2002 IOC cruise. Geochem. Geophys. Geosyst. 7, Q04M07. http://dx.doi.org/10.1029/2005GC000977.

Buck, C.S., Landing, W.M., Resing, J.A., Measures, C.I., 2010. The solubility and deposition of aerosol Fe and other trace elements in the North Atlantic Ocean: observations from the A16N CLIVAR/CO_2 repeat hydrography section. Mar. Chem. 120, 57–70. http://dx.doi.org/10.1016/j.marchem.2008.08.003.

Buck, C.S., Landing, W.M., Resing, J., 2013. Pacific Ocean aerosols: deposition and solubility of iron, aluminum, and other trace elements. Mar. Chem. 157, 117–130. http://dx.doi.org/10.1016/j.marchem.2013.09.005.

Buck, C.S., Aguilar-Islas, A.M., Marsay, C.M., Kadko, D., Landing, W.M., 2018. Trace element concentrations, elemental ratios, and enrichment factors observed in aerosol samples collected during the US GEOTRACES eastern Pacific Ocean transect (GP16). (this issue).

Celo, V., Dabek-Zlotorzynska, E., McCurdy, M., 2015. Chemical characterization of exhaust emissions from selected Canadian marine vessels: the case of trace metals and lanthanoids. Environ. Sci. Technol. 49, 5220–5226. http://dx.doi.org/10.1021/acs.est.5b00127.

Chance, R., Jickells, T.D., Baker, A.R., 2015. Atmospheric trace metal concentrations, solubility and deposition fluxes in remote marine air over the south-east Atlantic. Mar. Chem. 177, 45–56. http://dx.doi.org/10.1016/j.marchem.2015.06.028.

Chen, L., Duce, R.A., 1983. The sources of sulfate, vanadium and mineral matter in aerosol particles over Bermuda. Atmos. Environ. 17, 2055–2064. http://dx.doi.org/10.1016/0004-6981(83)90362-1.

Chester, R., Murphy, K.J.T., Lin, F.J., Berry, A.S., Bradshaw, G.A., Corcoran, P.A., 1993. Factors controlling the solubilities of trace metals from non-remote aerosols deposited to the sea surface by the "dry" deposition mode. Mar. Chem. 42, 107–126. http://dx.doi.org/10.1016/0304-4203(93)90241-F.

Chester, R., Nimmo, M., Fones, G.R., Keyse, S., Zhang, Z., 2000. Trace metal chemistry of particulate aerosols from the UK mainland coastal rim of the NE Irish sea. Atmos. Environ. 34, 949–958. http://dx.doi.org/10.1016/S1352-2310(99)00234-4.

Comiso, J.C., 2012. Large decadal decline of the Arctic multiyear ice cover. J. Clim. 25, 1176–1193. http://dx.doi.org/10.1175/JCLI-D-11-00113.1.

Cottle, P., Strawbridge, K., McKendry, I., 2014. Long-range transport of Siberian wildfire smoke to British Columbia: lidar observations and air quality impacts. Atmos. Environ. 90, 71–77. http://dx.doi.org/10.1016/j.atmosenv.2014.03.005.

Davidson, C.I., Chu, L., Grimm, T.C., Nasta, M.A., Qamoos, M.P., 1981. Wet and dry deposition of trace elements onto the Greenland ice sheet. Atmos. Environ. 15, 1429–1437. http://dx.doi.org/10.1016/0004-6981(81)90349-8.

Davidson, C.I., Santhanam, S., Fortmann, R.C., Marvin, P.O., 1985. Atmospheric transport and deposition of trace elements onto the Greenland Ice Sheet. Atmos. Environ. 19, 2065–2081. http://dx.doi.org/10.1016/0004-6981(85)90115-5.

Desboeufs, K.V., Sofikitis, A., Losno, R., Colin, J.L., Ausset, P., 2005. Dissolution and solubility of trace metals from natural and anthropogenic aerosol particulate matter. Chemosphere 58, 195–203. http://dx.doi.org/10.1016/j.chemosphere.2004.02.025.

Dibb, J.E., Meeker, L.D., Finkel, R.C., Southon, J.R., Caffee, M.W., Barrie, L.A., 1994. Estimation of stratospheric input to the Arctic troposphere: ^{7}Be and ^{10}Be in aerosols at Alert, Canada. J. Geophys. Res. Atmos. 99, 12,855–12,864. http://dx.doi.org/10.1029/94JD00742.

Duce, R.A., Liss, P.S., Merrill, J.T., Atlas, E.L., Buat-Menard, P., Hicks, B.B., Miller, J.M., Prospero, J.M., Arimoto, R., Church, T.M., Ellis, W., Galloway, J.N., Hansen, L., Jickells, T.D., Knap, A.H., Reinhardt, K.H., Schneider, B., Soudine, A., Tokos, J.J., Tsunogai, S., Wollast, R., Zhou, M., 1991. The atmospheric input of trace species to the world ocean. Glob. Biogeochem. Cycles 5, 193–259. http://dx.doi.org/10.1029/91GB01778.

Duggen, S., Olgun, N., Croot, P., Hoffmann, L., Dietze, H., Teschner, C., 2010. The role of airborne volcanic ash for the surface ocean biogeochemical iron-cycle: a review. Biogeosciences 7, 827–844. http://dx.doi.org/10.5194/bg-7-827-2010.

Fomba, K.W., Müller, K., van Pinxteren, D., Herrmann, H., 2013. Aerosol size-resolved trace metal composition in remote northern tropical Atlantic marine environment: case study Cape Verde islands. Atmos. Chem. Phys. 13, 4801–4814. http://dx.doi.org/10.5194/acp-13-4801-2013.

Gelado-Caballero, M.D., López-García, P., Prieto, S., Patey, M.D., Collado, C., Hérnández-Brito, J.J., 2012. Long-term aerosol measurements in Gran Canaria, Canary Islands: particle concentration, sources and elemental composition. J. Geophys. Res. Atmos. 117, D03304. http://dx.doi.org/10.1029/2011JD016646.

Gong, S.L., Barrie, L.A., 2005. Trends of heavy metal components in the Arctic aerosols and their relationship to the emissions in the Northern Hemisphere. Sci. Total Environ. 342, 175–183. http://dx.doi.org/10.1016/j.scitotenv.2004.12.031.

Guo, L., Chen, Y., Wang, F., Meng, X., Xu, Z., Zhuang, G., 2014. Effects of Asian dust on the atmospheric input of trace elements to the East China Sea. Mar. Chem. 163, 19–27. http://dx.doi.org/10.1016/j.marchem.2014.04.003.

Helmers, E., Rutgers van der Loeff, M.M., 1993. Lead and aluminum in Atlantic surface waters (50°N to 50°S) reflecting anthropogenic and natural sources in the eolian transport. J. Geophys. Res. Oceans 98, 20,261–20,273. http://dx.doi.org/10.1029/93JC01623.

Hirdman, D., Sodemann, H., Eckhardt, S., Burkhart, J.F., Jefferson, A., Mefford, T., Quinn, P.K., Sharma, S., Ström, J., Stohl, A., 2010. Source identification of short-lived air pollutants in the Arctic using statistical analysis of measurement data and particle dispersion model output. Atmos. Chem. Phys. 10, 669–693. http://dx.doi.org/10.5194/acp-10-669-2010.

Ittekkot, V., 1993. The abiotically driven biological pump in the ocean and short-term fluctuations in atmospheric CO_2 contents. Glob. Planet. Chang. 8, 17–25. http://dx.doi.org/10.1016/0921-8181(93)90060-2.

Jickells, T.D., An, Z.S., Andersen, K.K., Baker, A.R., Bergametti, G., Brooks, N., Cao, J.J., Boyd, P.W., Duce, R.A., Hunter, K.A., Kawahata, H., Kubilay, N., LaRoche, J., Liss, P.S., Mahowald, N., Prospero, J.M., Ridgwell, A.J., Tegen, I., Torres, R., 2005. Global iron connections between desert dust, ocean biogeochemistry, and climate. Science 308, 67–71. http://dx.doi.org/10.1126/science.1105959. (80-.).

Jones, M.T., Gislason, S.R., 2008. Rapid releases of metal salts and nutrients following the deposition of volcanic ash into aqueous environments. Geochim. Cosmochim. Acta 72, 3661–3680. http://dx.doi.org/10.1016/j.gca.2008.05.030.

Kadko, D., Prospero, J., 2011. Deposition of ^{7}Be to Bermuda and the regional ocean: environmental factors affecting estimates of atmospheric flux to the ocean. J. Geophys. Res. Oceans 116, C02013. http://dx.doi.org/10.1029/2010JC006629.

Kadko, D., Landing, W.M., Shelley, R.U., 2015. A novel tracer technique to quantify the atmospheric flux of trace elements to remote ocean regions. J. Geophys. Res. Oceans 120, 848–858. http://dx.doi.org/10.1002/2014JC010314.

Kadko, D., Galfond, B., Landing, W.M., Shelley, R.U., 2016. Determining the pathways, fate, and flux of atmospherically derived trace elements in the Arctic ocean/ice system. Mar. Chem. 182, 38–50. http://dx.doi.org/10.1016/j.marchem.2016.04.006.

Klunder, M.B., Bauch, D., Laan, P., de Baar, H.J.W., van Heuven, S., Ober, S., 2012. Dissolved iron in the Arctic shelf seas and surface waters of the central Arctic Ocean: impact of Arctic river water and ice-melt. J. Geophys. Res. Oceans 117, C01027. http://dx.doi.org/10.1029/2011JC007133.

Laing, J.R., Hopke, P.K., Hopke, E.F., Husain, L., Dutkiewicz, V.A., Paatero, J., Viisanen, Y., 2014a. Long-term particle measurements in Finnish Arctic: part I - chemical composition and trace metal solubility. Atmos. Environ. 88, 275–284. http://dx.doi.org/10.1016/j.atmosenv.2014.03.002.

Laing, J.R., Hopke, P.K., Hopke, E.F., Husain, L., Dutkiewicz, V.A., Paatero, J., Viisanen, Y., 2014b. Long-term particle measurements in Finnish Arctic: part II - trend analysis

and source location identification. Atmos. Environ. 88, 285–296. http://dx.doi.org/10.1016/j.atmosenv.2014.01.015.
Landsberger, S., Vermette, S.J., Barrie, L.A., 1990. Multielemental composition of the Arctic aerosol. J. Geophys. Res. Atmos. 95, 3509–3515. http://dx.doi.org/10.1029/JD095iD04p03509.
Lannefors, H., Heintzenberg, J., Hansson, H.-C., 1983. A comprehensive study of physical and chemical parameters of the Arctic summer aerosol; results from the Swedish expedition Ymer-80. Tellus B 35, 40–54. http://dx.doi.org/10.1111/j.1600-0889.1983.tb00006.x.
Law, K.S., Stohl, A., 2007. Arctic air pollution: origins and impacts. Science 315, 1537–1540. http://dx.doi.org/10.1126/science.1137695. (80-.).
Luo, C., Mahowald, N., Bond, T., Chuang, P.Y., Artaxo, P., Siefert, R., Chen, Y., Schauer, J., 2008. Combustion iron distribution and deposition. Glob. Biogeochem. Cycles 22, GB1012. http://dx.doi.org/10.1029/2007GB002964.
Macdonald, R.W., Harner, T., Fyfe, J., 2005. Recent climate change in the Arctic and its impact on contaminant pathways and interpretation of temporal trend data. Sci. Total Environ. 342, 5–86. http://dx.doi.org/10.1016/j.scitotenv.2004.12.059.
Maenhaut, W., Ducastel, G., Leck, C., Nilsson, E.D., Heintzenberg, J., 1996. Multi-elemental composition and sources of the high Arctic atmospheric aerosol during summer and autumn. Tellus B 48, 300–321. http://dx.doi.org/10.1034/j.1600-0889.1996.t01-1-00011.x.
Mahowald, N.M., Baker, A.R., Bergametti, G., Brooks, N., Duce, R.A., Jickells, T.D., Kubilay, N., Prospero, J.M., Tegen, I., 2005. Atmospheric global dust cycle and iron inputs to the ocean. Glob. Biogeochem. Cycles 19, GB4025. http://dx.doi.org/10.1029/2004GB002402.
Mahowald, N.M., Engelstaedter, S., Luo, C., Sealy, A., Artaxo, P., Benitez-Nelson, C., Bonnet, S., Chen, Y., Chuang, P.Y., Cohen, D.D., Dulac, F., Herut, B., Johansen, A.M., Kubilay, N., Losno, R., Maenhaut, W., Paytan, A., Prospero, J.M., Shank, L.M., Siefert, R.L., 2009. Atmospheric iron deposition: global distribution, variability, and human perturbations. Annu. Rev. Mar. Sci. 1, 245–278. http://dx.doi.org/10.1146/annurev.marine.010908.163727.
Middag, R., de Baar, H.J.W., Laan, P., Klunder, M.B., 2011. Fluvial and hydrothermal input of manganese into the Arctic Ocean. Geochim. Cosmochim. Acta 75, 2393–2408. http://dx.doi.org/10.1016/j.gca.2011.02.011.
Moore, J.K., Doney, S.C., Lindsay, K., 2004. Upper ocean ecosystem dynamics and iron cycling in a global three-dimensional model. Glob. Biogeochem. Cycles 18, GB4028. http://dx.doi.org/10.1029/2004GB002220.
Morton, P.L., Landing, W.M., Hsu, S.C., Milne, A., Aguilar-Islas, A.M., Baker, A.R., Bowie, A.R., Buck, C.S., Gao, Y., Gichuki, S., Hastings, M.G., Hatta, M., Johansen, A.M., Losno, R., Mead, C., Patey, M.D., Swarr, G., Vandermark, A., Zamora, L.M., 2013. Methods for the sampling and analysis of marine aerosols: results from the 2008 GEOTRACES aerosol intercalibration experiment. Limnol. Oceanogr. Methods 11, 62–78. http://dx.doi.org/10.4319/lom.2013.11.62.
Mukherjee, P., Gao, Y., Marsay, C., Buck, C., Landing, W.M., 2017. Characterization of the water soluble inorganic and organic species on aerosols in the Arctic troposphere during summer. Abstract #28434, ASLO 2017 Aquat. Sci. Meet., Honolulu, HI.
Nürnberg, D., Wollenburg, I., Dethleff, D., Eicken, H., Kassens, H., Letzig, T., Reimnitz, E., Thiede, J., 1994. Sediments in Arctic sea ice: implications for entrainment, transport and release. Mar. Geol. 119, 185–214. http://dx.doi.org/10.1016/0025-3227(94)90181-3.
Pacyna, J.M., Ottar, B., 1985. Transport and chemical composition of the summer aerosol in the Norwegian Arctic. Atmos. Environ. 19, 2109–2120. http://dx.doi.org/10.1016/0004-6981(85)90118-0.
Pacyna, J.M., Pacyna, E.G., 2001. An assessment of global and regional emissions of trace metals to the atmosphere from anthropogenic sources worldwide. Environ. Rev. 9, 269–298. http://dx.doi.org/10.1139/er-9-4-269.
Patey, M.D., Achterberg, E.P., Rijkenberg, M.J., Pearce, R., 2015. Aerosol time-series measurements over the tropical Northeast Atlantic Ocean: dust sources, elemental composition and mineralogy. Mar. Chem. 174, 103–119. http://dx.doi.org/10.1016/j.marchem.2015.06.004.
Peirson, D.H., Cawse, P.A., Cambray, R.S., 1974. Chemical uniformity of airborne particulate material, and a maritime effect. Nature 251, 675–679. http://dx.doi.org/10.1038/251675a0.
Rahn, K.A., 1981. Atmospheric, riverine and oceanic sources of seven trace constituents to the Arctic Ocean. Atmos. Environ. 15, 1507–1516. http://dx.doi.org/10.1016/0004-6981(81)90359-0.
Rogan, N., Achterberg, E.P., Le Moigne, F.A.C., Marsay, C.M., Tagliabue, A., Williams, R.G., 2016. Volcanic ash as an oceanic iron source and sink. Geophys. Res. Lett. 43, 2732–2740. http://dx.doi.org/10.1002/2016GL067905.
Rolph, G., Stein, A., Stunder, B., 2017. Real-time Environmental Applications and Display sYstem: READY. Environ. Model. Softw. 95, 210–228. http://dx.doi.org/10.1016/j.envsoft.2017.06.025.
Shaw, G.E., 1995. The Arctic haze phenomenon. Bull. Am. Meteorol. Soc. 76, 2403–2413. http://dx.doi.org/10.1175/1520-0477(1995)076<2403:TAHP>2.0.CO;2.
Shelley, R.U., Morton, P.L., Landing, W.M., 2015. Elemental ratios and enrichment factors in aerosols from the US-GEOTRACES North Atlantic transects. Deep-Sea Res. II Top. Stud. Oceanogr. 116, 262–272. http://dx.doi.org/10.1016/j.dsr2.2014.12.005.
Shelley, R.U., Roca-Martí, M., Castrillejo, M., Masqué, P., Landing, W.M., Planquette, H., Sarthou, G., 2017. Quantification of trace element atmospheric deposition fluxes to the Atlantic Ocean (> 40°N; GEOVIDE, GEOTRACES GA01) during spring 2014. Deep-Sea Res. I Oceanogr. Res. Pap. 119, 34–49. http://dx.doi.org/10.1016/j.dsr.2016.11.010.
Shevchenko, V., Lisitzin, A., Vinogradova, A., Stein, R., 2003. Heavy metals in aerosols over the seas of the Russian Arctic. Sci. Total Environ. 306, 11–25. http://dx.doi.org/10.1016/S0048-9697(02)00481-3.
Sirois, A., Barrie, L.A., 1999. Arctic lower tropospheric aerosol trends and composition at Alert, Canada: 1980–1995. J. Geophys. Res. Atmos. 104, 11,599–11,618. http://dx.doi.org/10.1029/1999JD900077.
Stein, A.F., Draxler, R.R., Rolph, G.D., Stunder, B.J.B., Cohen, M.D., Ngan, F., 2015. NOAA's HYSPLIT atmospheric transport and dispersion modeling system. Bull. Am. Meteorol. Soc. 96, 2059–2077. http://dx.doi.org/10.1175/BAMS-D-14-00110.1.
Stohl, A., 2006. Characteristics of atmospheric transport into the Arctic troposphere. J. Geophys. Res. Atmos. 111, D11306. http://dx.doi.org/10.1029/2005JD006888.
Stohl, A., Andrews, E., Burkhart, J.F., Forster, C., Herber, A., Hoch, S.W., Kowal, D., Lunder, C., Mefford, T., Ogren, J.A., Sharma, S., Spichtinger, N., Stebel, K., Stone, R., Ström, J., Tørseth, K., Wehrli, C., Yttri, K.E., 2006. Pan-Arctic enhancements of light absorbing aerosol concentrations due to North American boreal forest fires during summer 2004. J. Geophys. Res. Atmos. 111, D22214. http://dx.doi.org/10.1029/2006JD007216.
Streibel, T., Schnelle-Kreis, J., Czech, H., Harndorf, H., Jakobi, G., Jokiniemi, J., Karg, E., Lintelmann, J., Matuschek, G., Michalke, B., Müller, L., Orasche, J., Passig, J., Radischat, C., Rabe, R., Reda, A., Rüger, C., Schwemer, T., Sippula, O., Stengel, B., Sklorz, M., Torvela, T., Weggler, B., Zimmermann, R., 2017. Aerosol emissions of a ship diesel engine operated with diesel fuel or heavy fuel oil. Environ. Sci. Pollut. Res. 24, 10,976–10,991. http://dx.doi.org/10.1007/s11356-016-6724-z.
Taylor, S.R., 1964. Abundance of chemical elements in the continental crust: a new table. Geochim. Cosmochim. Acta 28, 1273–1285. http://dx.doi.org/10.1016/0016-7037(64)90129-2.
Taylor, S.R., McLennan, S.M., 1995. The geochemical evolution of the continental crust. Rev. Geophys. 33, 241–265. http://dx.doi.org/10.1029/95RG00262.
Taylor, R.L., Semeniuk, D.M., Payne, C.D., Zhou, J., Tremblay, J.-É., Cullen, J.T., Maldonado, M.T., 2013. Colimitation by light, nitrate, and iron in the Beaufort Sea in late summer. J. Geophys. Res. Oceans 118, 3260–3277. http://dx.doi.org/10.1002/jgrc.20244.
Tunved, P., Ström, J., Krejci, R., 2013. Arctic aerosol life cycle: linking aerosol size distributions observed between 2000 and 2010 with air mass transport and precipitation at Zeppelin station, Ny-Ålesund, Svalbard. Atmos. Chem. Phys. 13, 3643–3660. http://dx.doi.org/10.5194/acp-13-3643-2013.
Vaughan, D.G., Comiso, J.C., Allison, I., Carrasco, J., Kaser, G., Kwok, R., Mote, P., Murray, T., Paul, F., Ren, J., Rignot, E., Solomina, O., Steffen, K., Zhang, T., 2013. Observations: Cryosphere. In: Stocker, T.F., Qin, D., Plattner, G.-K., Tignor, M., Allen, S.K., Boschung, J., Nauels, A., Xia, Y., Bex, V., Midgley, P.M. (Eds.), Climate Change 2013: The Physical Science Basis. Contribution of Working Group I to the Fifth Assessment Report of the Intergovernmental Panel on Climate Change. Cambridge University Press, Cambridge, UK and New York, NY, USA.
Viana, M., Amato, F., Alastuey, A., Querol, X., Moreno, T., Dos Santos, S.G., Herce, M.D., Fernández-Patier, R., 2009. Chemical tracers of particulate emissions from commercial shipping. Environ. Sci. Technol. 43, 7472–7477. http://dx.doi.org/10.1021/es901558t.
Wallace, L., Slonecker, T., 1997. Ambient air concentrations of fine ($PM_{2.5}$) manganese in U.S. national parks and in California and Canadian cities: the possible impact of adding MMT to unleaded gasoline. J. Air Waste Manage. Assoc. 47, 642–652. http://dx.doi.org/10.1080/10473289.1997.10463930.
Wang, S., Bailey, D., Lindsay, K., Moore, J.K., Holland, M., 2014. Impact of sea ice on the marine iron cycle and phytoplankton productivity. Biogeosciences 11, 4713–4731. http://dx.doi.org/10.5194/bg-11-4713-2014.
Zhan, J., Gao, Y., 2014. Impact of summertime anthropogenic emissions on atmospheric black carbon at Ny-Ålesund in the Arctic. Polar Res. 33, 21821. http://dx.doi.org/10.3402/polar.v33.21821.
Zhan, J., Gao, Y., Li, W., Chen, L., Lin, H., Lin, Q., 2014. Effects of ship emissions on summertime aerosols at Ny–Alesund in the Arctic. Atmos. Pollut. Res. 5, 500–510. http://dx.doi.org/10.5094/APR.2014.059.